Journal of Molecular and Cellular Cardiology 59 (2013) 76–85

Contents lists available at SciVerse ScienceDirect

Journal of Molecular and Cellular Cardiology

journal homepage: www.elsevier.com/locate/yjmcc

Original article

Global metabolomic analysis of heart tissue in a hamster model for dilated cardiomyopathy

Keiko Maekawa [a,1], Akiyoshi Hirayama [b,1], Yuko Iwata [c,1], Yoko Tajima [a], Tomoko Nishimaki-Mogami [a], Shoko Sugawara [b], Noriko Ueno [a], Hiroshi Abe [b], Masaki Ishikawa [a], Mayumi Murayama [a], Yumiko Matsuzawa [a], Hiroki Nakanishi [a,d], Kazutaka Ikeda [b], Makoto Arita [a,e], Ryo Taguchi [a,f], Naoto Minamino [c], Shigeo Wakabayashi [c], Tomoyoshi Soga [b,*,1], Yoshiro Saito [a,**,1]

[a] Project Team for Disease Metabolomics, National Institute of Health Sciences, Tokyo 158-8501, Japan
[b] Institute for Advanced Biosciences, Keio University, Tsuruoka, Yamagata 997-0052, Japan
[c] National Cerebral and Cardiovascular Center Research Institute, Suita, Osaka 565-8565, Japan
[d] Bioscience and Research Center, Akita University, Akita 010-8543, Japan
[e] Department of Health Chemistry, Graduate School of Pharmaceutical Sciences, University of Tokyo, Tokyo 113-0033, Japan
[f] College of Life and Health Sciences, Chubu University, Kasugai, Aichi 487-8501, Japan

ARTICLE INFO

Article history:
Received 19 September 2012
Received in revised form 8 January 2013
Accepted 6 February 2013
Available online 20 February 2013

Keywords:
Dilated cardiomyopathy
Hamster model
Metabolomics
Oxidative stress
Phospholipid alteration

ABSTRACT

Dilated cardiomyopathy (DCM), a common cause of heart failure, is characterized by cardiac dilation and reduced left ventricular ejection fraction, but the underlying mechanisms remain unclear. To investigate the mechanistic basis, we performed global metabolomic analysis of myocardial tissues from the left ventricles of J2N-k cardiomyopathic hamsters. This model exhibits symptoms similar to those of human DCM, owing to the deletion of the δ-sarcoglycan gene. Charged and lipid metabolites were measured by capillary electrophoresis mass spectrometry (MS) and liquid chromatography MS(/MS), respectively, and J2N-k hamsters were compared with J2N-n healthy controls at 4 (presymptomatic phase) and 16 weeks (symptomatic) of age. Disturbances in membrane phospholipid homeostasis were initiated during the presymptomatic phase. Significantly different levels of charged metabolites, occurring mainly in the symptomatic phase, were mapped to primary metabolic pathways. Reduced levels of metabolites in glycolysis, the pentose phosphate pathway, and the tricarboxylic acid cycle, together with large decreases in major triacylglycerol levels, suggested that decreased energy production leads to cardiac contractile dysfunction in the symptomatic phase. A mild reduction in glutathione and a compensatory increase in ophthalmate levels suggest increased oxidative stress in diseased tissues, which was confirmed by histochemical staining. Increased levels of 4 eicosanoids, including prostaglandin (PG) E_2 and 6-keto-$PGF_{1\alpha}$, in the symptomatic phase suggested activation of the protective response pathways. These results provide mechanistic insights into DCM pathogenesis and may help identify new targets for therapeutic intervention and diagnosis.

1. Introduction

Dilated cardiomyopathy (DCM), a common cause of heart failure and a prevalent cardiomyopathy [1], is characterized by left ventricular dilation, impaired cardiac pump function, and a thin cardiac wall, which result in severe contractile dysfunction. β-Blockers constitute a common treatment [2], but severely affected patients may undergo heart transplantation or implantation of left ventricular assist devices. While the underlying etiological factors remain largely unknown, and both familial and non-familial factors are associated with DCM, some proposed disease mechanisms include coronary artery disease, genetic mutation, and viral infection [3]. Mutations in sarcomeric and cytoskeletal genes cause hypertrophic and dilated cardiomyopathies, respectively [4]. Some familial DCM cases are caused by mutations in genes encoding components of the dystrophin–glycoprotein complex (DGC), which spans the sarcolemma linking the extracellular matrix and cytoskeleton and provides mechanical strength for contraction [5]. Mutations in dystrophin, a major cytoskeletal component of the DGC, lead to a high incidence of X-linked DCM in patients with

* Correspondence to: T. Soga, Institute for Advanced Biosciences, Keio University, 246-2 Mizukami, Kakuganji, Tsuruoka, Yamagata 997-0052, Japan. Tel.: +81 235 29 0528; fax: +81 235 29 0574.
** Correspondence to: Y. Saito, Project Team for Disease Metabolomics, National Institute of Health Sciences, 1-18-1 Kamiyoga, Setagaya-ku, Tokyo 158-8501, Japan. Tel.: +81 3 3700 9528; fax: +81 3 3700 9788.
E-mail addresses: soga@sfc.keio.ac.jp (T. Soga), yoshiro@nihs.go.jp (Y. Saito).
[1] Contributed equally to this work.

0022-2828/$ – see front matter © 2013 Elsevier Ltd. All rights reserved.
http://dx.doi.org/10.1016/j.yjmcc.2013.02.008

Duchenne or Becker muscular dystrophy. Mutations in other DGC genes, including *δ-sarcoglycan*, are also associated with human DCM [1].

Oxidative stress is also reported to be involved in DCM pathogenesis. Patients with DCM exhibit increased plasma glutathione levels and lipid peroxidation products such as malondialdehyde [6], and total plasma peroxide levels are inversely correlated with the cardiac ejection fraction [7]. However, a contrasting study found that human left ventricular DCM tissue showed normal glutathione peroxidase and superoxide dismutase activities and malondialdehyde levels similar to those found in healthy control tissue [8]. Thus, the role of oxidative stress in DCM pathogenesis remains to be elucidated.

Animal models with a pathophysiology similar to human DCM are useful for investigating pathogenic mechanisms. A J2N-k DCM hamster and J2N-n control line were established by repeated sib mating of J2N(N8), produced by cross-breeding BIO14.6 cardiomyopathic and normal golden hamsters [9]. J2N-k hamsters are deficient in δ-sarcoglycan and are an animal model of human limb-girdle muscular dystrophy–associated cardiomyopathy. They begin showing heart tissue fibrosis and exhibit moderate cardiac dysfunction at 8–9 weeks of age. At 20 weeks, J2N-k hamsters exhibit considerable fibrosis, a reduced number of cardiomyocytes, and hypertrophic changes in the remaining cardiomyocytes; no such changes occur in J2N-n heart tissues [9]. Accordingly, the life span of J2N-k hamsters (ca. 298 days) is much shorter than that of J2N-n hamsters (ca. 788 days). Besides the *δ-sarcoglycan* gene, J2N-k and J2N-n hamsters have very similar genetic backgrounds. Since mutations in *δ-sarcoglycan* are also detected in DCM patients, J2N-k hamsters are an ideal DCM disease model.

To gain an insight into the DCM in metabolic pathway basis, we performed global metabolomic analysis of myocardial tissues from the left ventricles of J2N-k and J2N-n hamsters. Capillary electrophoresis-time-of-flight mass spectrometry (CE-TOFMS) [10] and liquid chromatography (LC)-TOFMS or triple quadrupole MS/MS were used to measure levels of charged (e.g., amino acids) and lipid (e.g., phospholipids) metabolites, respectively. We identified significant changes in several metabolite levels in age-matched J2N-k and J2N-n hamsters.

2. Methods

2.1. Animals

Male 3- and 15-week-old J2N-k cardiomyopathic hamsters and age-matched J2N-n controls were purchased from Nihon SLC Inc. (Hamamatsu, Japan). All animals were maintained in a specific pathogen-free facility under controlled conditions (20–24 °C and 40–70% humidity) with a 12-h light cycle and were given free access to standard laboratory rat chow (MF, Oriental Yeast, Tokyo, Japan) and tap water. After 1 week of habituation, 4- and 16-week-old animals were anesthetized by intraperitoneal injection of pentobarbital (Dainippon Sumitomo Pharma, Osaka, Japan) at a dose of 50 mg/kg, and the left ventricle was excised. The isolated tissue was processed for either histological analysis (N=4) or for metabolomic and western blot analysis (N=7). For metabolomic analysis, tissue was randomly divided into 2 samples and minced on ice to measure charged and lipid metabolites. The tissue samples were weighed and snap frozen in liquid nitrogen before being stored at −80 °C. All animal experiments were performed in accordance with the Guide for the Care and Use of Laboratory Animals published by the US National Institutes of Health (NIH Publication No. 85-23, revised 1996) and the Guidelines for Animal Experimentation and under the control of the Ethics Committee of Animal Care and Experimentation of the National Cerebral and Cardiovascular Center, Japan (Approval number, 12056).

2.2. Echocardiography and histochemical staining

Cardiac function was assessed by echocardiography measurements as shown in the supplementary information. Following this procedure, J2N-k and J2N-n hamsters were sacrificed as described above, and ventricle tissue (from both hamster lines) was processed for Masson's trichrome staining to detect fibrosis, 4-hydroxynonenal (4-HNE) staining to estimate lipid peroxidation [11], and dihydroethidium (DHE) staining to approximate superoxide production [12] as described in the supplementary information.

2.3. Metabolite extraction and quantification

Detailed information regarding the extraction and quantification of charged and lipid metabolites has been provided in the supplementary information. Briefly, charged metabolites were extracted by homogenizing myocardial tissue in methanol and subjected to CE-TOFMS, as previously described [10,13,14]. Lipid metabolite extraction was performed using the Bligh and Dyer method [15] with minor modifications. Lower organic and upper aqueous layers were analyzed by LC-TOFMS and LC-MS/MS for phospholipids/sphingolipids/triacylglycerols and oxidative fatty acids, respectively. Structural analysis of phospholipids (PLs) and sphingomyelins (SMs) was performed as previously described [16].

2.4. Data analysis

Datasets obtained from CE-TOFMS were processed using our proprietary software, MasterHands [17] as shown in the supplementary information. Hydrophilic metabolite concentrations have been provided as the amount of metabolite (μmol) per gram of tissue.

LC-TOFMS data were processed using the 2DICAL software (Mitsui Knowledge Industry, Tokyo, Japan) [18] as described in the supplementary information. Extracted ion peaks were normalized using internal standards (ISs). Metabolites eluting from 0.1 to 37.5 min and from 37.5 to 60 min for LC were normalized to 1, 2-dipalmitoyl-[$^2H_6$]-sn-glycero-3-phosphocholine (16:0-16:0PC-d6; Larodan Fine Chemicals, Malmo, Sweden) and 1,2-caprylin-3-linolein, respectively. Some oxidative fatty acids were quantified using commercially available standards.

2.5. Statistical and multiple classification analyses

Student's *t*-test was used for two-class comparisons between J2N-n and J2N-k at each growth stage (4 and 16 weeks), and $p<0.05$ was deemed as statistically significant. The multiple testing correction was not applied since metabolite levels are not exclusive but rather related with each other, and we focused on revealing overall metabolic changes (such as pathways or metabolite groups) in the cardiomyocytes from J2N-k hamsters compared to J2N-n cardiomyocytes. In addition, data were imported into the SIMCA-P+ software (Version 12.0; Umetrics, Umeå, Sweden), pareto-scaled, and subjected to principal component analysis (PCA; short explanation is provided in the supplementary information). Cluster analysis and heatmap representations were obtained using the Spotfire software (Version 7.1; TIBCO, MA, USA).

3. Results

3.1. Cardiac function and pathophysiology of J2N-n and J2N-k hamsters

In this study, the 4- and 16-weeks of ages were selected as DCM presymptomatic and symptomatic phases for J2N-k (and its control J2N-n) hamsters according to the previous paper [9]. First, we examined cardiac function of both hamsters at these time points. Echocardiograph measurements of J2N-k hamsters at 16 weeks revealed a significant increase in the internal diameter of the left ventricle (LVID) during both diastolic and systolic states; however, this

Table 1
Summary of echocardiographic analysis.

		4 weeks	4 weeks	16 weeks	16 weeks	
		J2N-n	J2N-k	J2N-n	J2N-k	*p* values
LVIDd	mm	3.10 ± 0.05	2.89 ± 0.23	3.80 ± 0.36	5.07 ± 0.26	0.0291*
LVIDs	mm	1.49 ± 0.10	1.21 ± 0.20	2.06 ± 0.18	3.64 ± 0.21	0.0013**
LVPWd	mm	1.85 ± 0.18	1.82 ± 0.31	2.09 ± 0.30	1.77 ± 0.09	0.3487
LVPWs	mm	2.22 ± 0.11	2.08 ± 0.22	2.28 ± 0.27	1.95 ± 0.13	0.3285
EF	%	77.64 ± 1.43	83.68 ± 3.07	77.64 ± 1.44	54.46 ± 1.04	<0.0001***
FS	%	51.80 ± 3.53	58.41 ± 5.63	45.62 ± 1.41	28.35 ± 0.60	<0.0001***
LV VOLd	μL	38.03 ± 1.46	32.81 ± 6.57	64.50 ± 14.69	123.70 ± 15.58	0.0327*
LV VOLs	μL	6.13 ± 1.08	4.01 ± 1.53	14.31 ± 2.94	56.69 ± 8.27	0.0029**

LVIDd, left ventricular internal diameter in diastole; LVIDs, left ventricular internal diameter in systole; LVPWd, left ventricular posterior wall in diastole; LVPWs, left ventricular posterior wall in systole; EF, ejection fraction; FS, fractional shortening (given by (LVIDd-LVIDs)/LVIDd × 100); LV VOLd, left ventricular volume in diastole; LV VOLs, left ventricular volume in systole. *p* values are analyzed between 16 week-old J2N-k and J2N-n hamsters. In 4 week-old hamsters, the *p* values are not significant.
* $p<0.05$.
** $p<0.005$.
*** $p<0.0001$.

was not observed at 4 weeks of age (Table 1). In addition, markedly reduced ejection fractions and fractional shortening were revealed at 16 weeks (Table 1 and Supplementary Fig. 1). Extensive fibrosis was observed in J2N-k hamsters at 16 weeks (compared to the J2N-n) by Masson's trichrome staining (Supplementary Fig. 2). No fibrosis was observed at 4 weeks. Thus, no obvious pathophysiological change was observed at 4 weeks, although DCM was obvious at 16 weeks in J2N-k hamsters.

3.2. Profiling of charged metabolites measured by CE-TOFMS

Charged metabolite levels were quantified absolutely using standard chemicals for each metabolite, whereas lipid metabolite levels were quantified relatively as ratios of ion counts (peak height) of each metabolite to those of the internal standard, with the exception of some oxidative fatty acids. Therefore, statistical analyses of charged and lipid metabolites were carried out separately.

A total of 180 charged metabolites were identified and quantified by the CE-TOFMS method (Supplementary Table 2). Using a whole dataset of quantified metabolites, we performed a PCA (Supplementary Fig. 3) in order to understand the similarities/dissimilarities of 4 animal groups regarding variations in metabolite levels. From the PCA score plot, DCM and control hamsters at 16 weeks (but not at 4 weeks) were separated in the first 2 principal components. This analysis indicates that the profiles of charged metabolites reflect the metabolic differences caused by disease progression.

Next, Student's *t*-test was used to examine DCM-associated metabolic changes (Supplementary Table 2). Using a *p*-value threshold of 0.01 to generate a heatmap (Fig. 1A), the levels of 15 metabolites were found to differ between J2N-k and J2N-n hamsters at 4 weeks; specifically, the level of 12 metabolites increased and 3 metabolites decreased in J2N-k hamsters. At the symptomatic phase (16 weeks), 62 metabolites were detected at different levels ($p<0.01$) in J2N-k and J2N-n hamsters (Fig. 1B), including 10 metabolites that also showed significant differences in the presymptomatic phase (4 weeks; 2-aminobutyrate (2-AB), citrulline, guanidinoacetate, hypotaurine, methionine, *N*-acetylaspartate, ophthalmate, ornithine, threonine, and trigonelline). Of the 62 metabolites showing variation, the levels of 26 increased and 36 decreased in the J2N-k hamsters. Most of these metabolites are components of primary metabolic pathways such as glycolysis, the pentose phosphate pathway, the tricarboxylic acid (TCA) cycle, the glutathione biosynthesis pathway, and the urea cycle.

3.3. Energy metabolism

J2N-k myocardial tissues from 16-week-old animals exhibited changes in the levels of metabolic intermediates involved in energy metabolism. The concentrations of several intermediates involved in glycolysis, such as glucose 6-phopshate (G6P; levels of J2N-k/J2N-n = 0.5-fold, $p=5.9\times10^{-5}$), dihydroxyacetone phosphate (DHAP; 0.6-fold, $p=1.4\times10^{-3}$), and acetyl CoA (0.3-fold, $p=1.1\times10^{-5}$), were significantly reduced at 16 weeks but not at 4 weeks (Fig. 2).

Significantly decreased levels of the TCA cycle intermediates, isocitrate (0.6-fold, $p=1.5\times10^{-6}$) and malate (0.7-fold, $p=2.5\times10^{-3}$), were also observed in myocardial tissues from 16-week-old J2N-k hamsters. Decreased protein levels of aconitase 2, which catalyzes citrate to isocitrate via *cis*-aconitate, were observed at 16 weeks in the J2N-k, suggesting decreased TCA cycle activity (Supplementary Fig. 4). These results suggest that the levels of metabolites involved in glycolysis and the TCA cycle energy pathways are attenuated in J2N-k cardiomyopathic tissue during the symptomatic phase.

3.4. Glutathione biosynthesis pathway

The ophthalmate and 2-AB levels were significantly higher in J2N-k myocardial tissues than in J2N-n control tissue at both the presymptomatic (1.4-fold, $p=2.6\times10^{-3}$; 2.2-fold, $p=6.9\times10^{-5}$, respectively) and symptomatic (2.3-fold, $p=3.9\times10^{-7}$; 4.2-fold, $p=2.2\times10^{-9}$, respectively) phases (Fig. 3). 2-AB is metabolized to ophthalmate via γ-Glu-2-AB through a 2-step reaction and then catalyzed sequentially by γ-glutamylcysteine synthetase and glutathione synthetase [10]. In contrast, γ-Glu-Cys and glutathione (GSH) concentrations are decreased at 16 weeks (0.2-fold, $p=7.9\times10^{-3}$; 0.8-fold, $p=2.0\times10^{-2}$, respectively). These data suggest that upregulation of the GSH biosynthetic pathway is associated with DCM progression. Consistent with this observation, intracellular levels of glycine (1.3-fold, $p=1.2\times10^{-5}$), methionine (1.3-fold, $p=2.9\times10^{-5}$), and *S*-adenosylhomocysteine (SAH; 1.2-fold, $p=2.4\times10^{-2}$) were elevated in J2N-k hamsters at 16 weeks. In contrast, *S*-adenosylmethionine (SAM; 0.9-fold, $p=3.2\times10^{-2}$) levels were reduced at the symptomatic-phase in J2N-k hamsters.

Taurine levels did not differ significantly between the 2 genotypes, although increased concentrations of its precursor, hypotaurine, were observed in J2N-k hamsters at both 4 weeks (1.6-fold, $p=6.9\times10^{-5}$) and 16 weeks (3.4-fold, $p=1.6\times10^{-9}$).

3.5. Urea cycle

The levels of most urea cycle intermediates significantly differed between myocardial tissues from J2N-k and J2N-n at 16 weeks (Fig. 4). The levels of arginine (0.7-fold, $p=3.2\times10^{-5}$), citrulline (0.6-fold, $p=2.0\times10^{-5}$), and argininosuccinate (0.4-fold, $p=6.3\times10^{-4}$) were significantly reduced in J2N-k hamsters. In contrast, ornithine levels (1.8-fold, $p=8.2\times10^{-8}$) were significantly increased. At 4 weeks, a

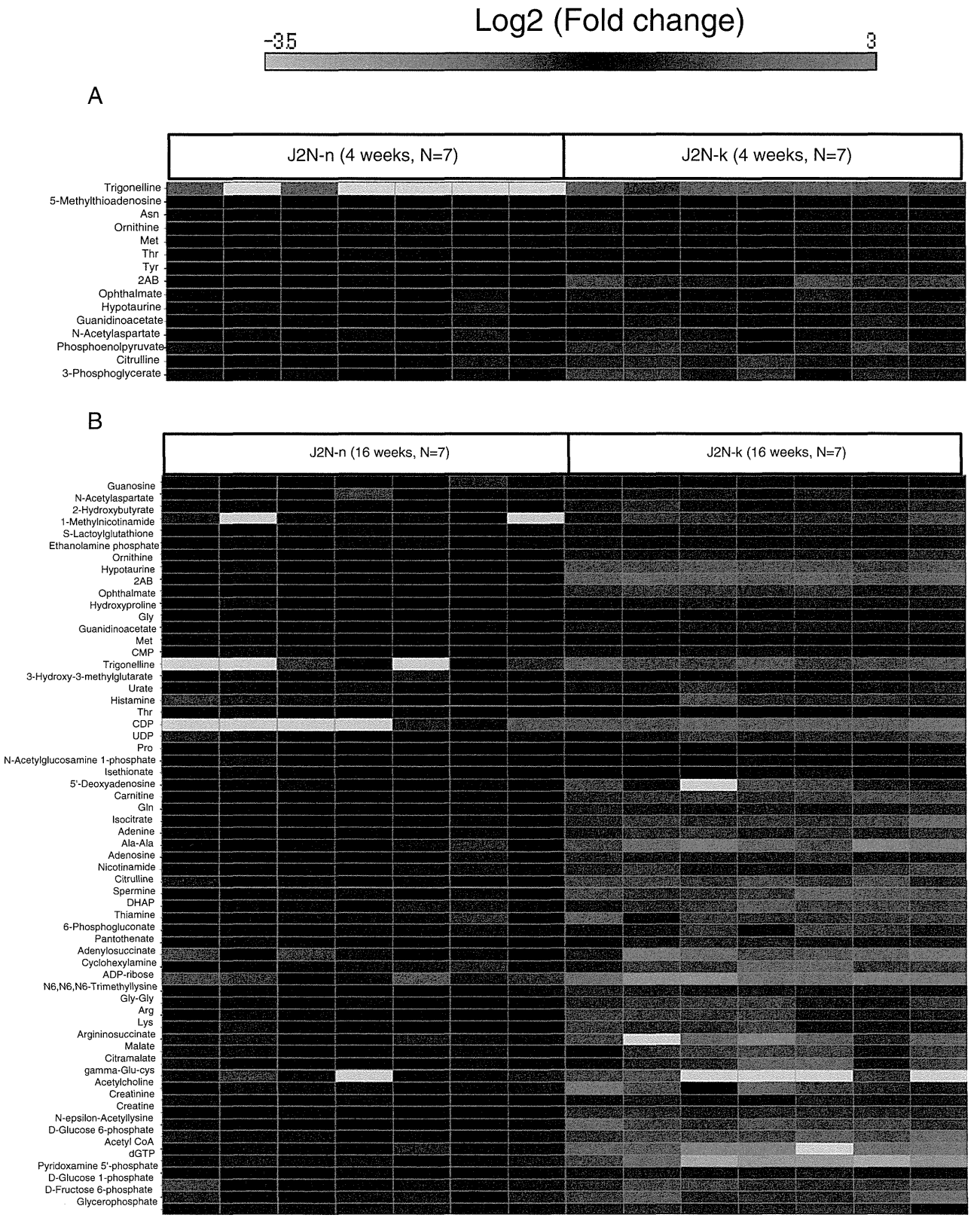

Fig. 1. Heatmap showing charged metabolites in myocardial tissues from J2N-n and J2N-k hamsters at (A) 4 weeks and (B) 16 weeks ($n=7$ in all groups). Fold changes in the amounts of each metabolite in individual J2N-k samples, relative to the average amounts in J2N-n at either 4 or 16 weeks are represented as the log2 ratio. Light gray cells indicate that metabolites were not detected in those samples. Fifteen (at 4 weeks) and sixty-two (at 16 weeks) charged metabolites that showed different levels ($p<0.01$) at each time point are shown, excluding Glu–Glu at 16 weeks, which was not detected in all J2N-n samples.

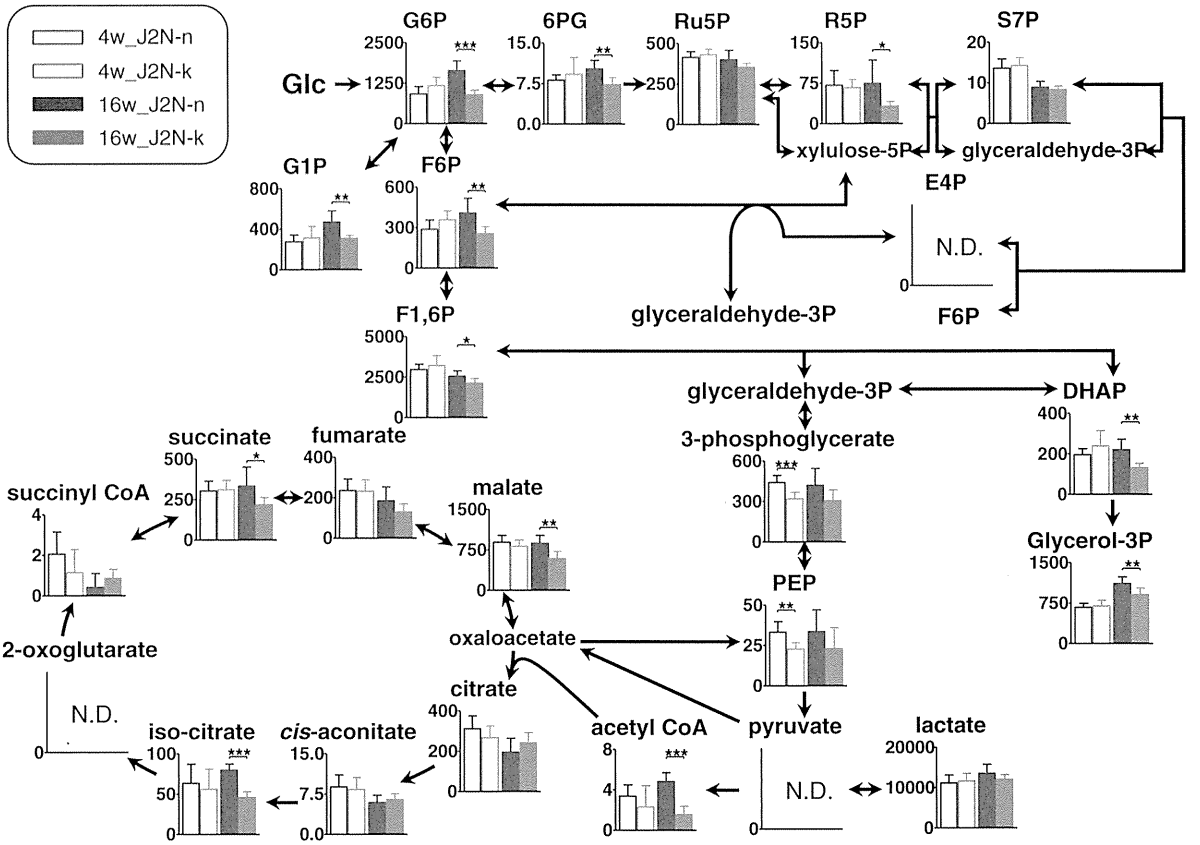

Fig. 2. Metabolome pathway map of quantified charged metabolites, including components of the glycolytic pathway, pentose phosphate pathway, and TCA cycle in J2N-n and J2N-k hamsters at 4 and 16 weeks (4w and 16w). The columns represent average concentrations (nmol/g tissue), and the error bars indicate SD. $^{*}p<0.05$; $^{**}p<0.01$; $^{***}p<0.001$; and N.D., not detected.

significant increase in ornithine levels (1.4-fold, $p=2.3\times10^{-4}$) and a decrease in citrulline levels (0.7-fold, $p=1.1\times10^{-3}$) were also observed in J2N-k hamsters.

3.6. Profiling of lipid metabolites measured by LC-TOFMS

LC-TOFMS detected 1173 peaks and 277 peaks in the positive and negative ion modes, respectively. Relative quantification of the identified metabolites is shown in Supplementary Table 3.

Next, the data were processed for PCA. In the positive ion mode, the 1173 peaks (including unidentified metabolites) were divided into 2 groups on the basis of their retention time (RT): 0.1–37.5 min RT (671 peaks; containing lysophospholipids [lysoPLs], diacylglycerols [DAGs], PLs, SMs, and ceramides [Cers]) and 37.5–60 min RT (502 peaks; containing triacylglycerols [TAGs] and cholesterol esters [ChEs]; Supplementary Fig. 5). PCA was performed separately for each group since PLs and TAGs are the 2 major classes of lipid metabolites in this mode (Supplementary Fig. 6). Distinct clustering of metabolites among the 4 groups (i.e., 4- or 16-week-old J2N-n and J2N-k hamsters) was observed in the data obtained using both positive (0.1–37.5 min RT; Supplementary Fig. 6A) and negative ion modes (data not shown). In contrast, for the second group of metabolites identified in the positive ion mode (37.5–60 min RT), poor discrimination was obtained between all tissue samples (from 4- and 16-week-old J2N-k and J2N-n hamsters) (Supplementary Fig. 6B). These results suggest that the lipid metabolites that were eluted from 0.1 to 37.5 min include candidates for identifying DCM and healthy tissues, even in the presymptomatic phase (4 weeks). Using a p-value threshold of 0.01 for the heatmap, the levels of 34 and 68 metabolites were found to differ between J2N-n and J2N-k hamsters at 4 and 16 weeks, respectively, with 15 overlapping metabolites (Fig. 5).

3.7. Myocardial lipid levels are significantly different in J2N-k and J2N-n tissues

PLs are important components of heart membranes. When focusing on phosphatidylcholine (PC), the levels of many species, most of which contained unsaturated fatty acids, increased in J2N-k compared with J2N-n at the presymptomatic phase (4 weeks). Some of these PC species remained upregulated in the symptomatic phase (16 weeks) (Fig. 5, Supplementary Table 3), including 18:0/20:4PC (1.4-fold, $p=5.4\times10^{-4}$; 1.6-fold, $p=2.0\times10^{-5}$; at 4 and 16 weeks, respectively) and 18:0/22:6PC (1.7-fold, $p=7.0\times10^{-5}$ and 1.7-fold, $p=2.0\times10^{-5}$; at 4 and 16 weeks, respectively). In contrast, levels of several PC species containing linoleic acid (18:2), such as 18:2/18:2PC (0.8-fold, $p=9.4\times10^{-3}$), were reduced at 16 weeks. As for lyso species, a significant increase in the level of 18:0 lyso PC (LPC; 1.4-fold, $p=9.5\times10^{-4}$) was observed in J2N-k at 16 weeks but not at 4 weeks.

Regarding phosphatidylethanolamine (PE) and plasmalogen PE (pPE), the levels of several species containing 22:5 and 22:6 (docosahexaenoic acid, DHA), such as 18:0/22:6PE (1.3-fold, $p=6.1\times10^{-3}$), increased in J2N-k compared with J2N-n hamsters at 4 weeks, although their increase was almost diminished at 16 weeks. At 16 weeks, many species (11 PEs and 8 pPEs) were decreased in J2N-k tissues (Fig. 5, Supplementary Table 3), although 3 PE and 2 pPE species were increased in J2N-k tissues. Notably, species containing linoleic acid (18:2) or eicosapentaenoic acid (EPA; 20:5),

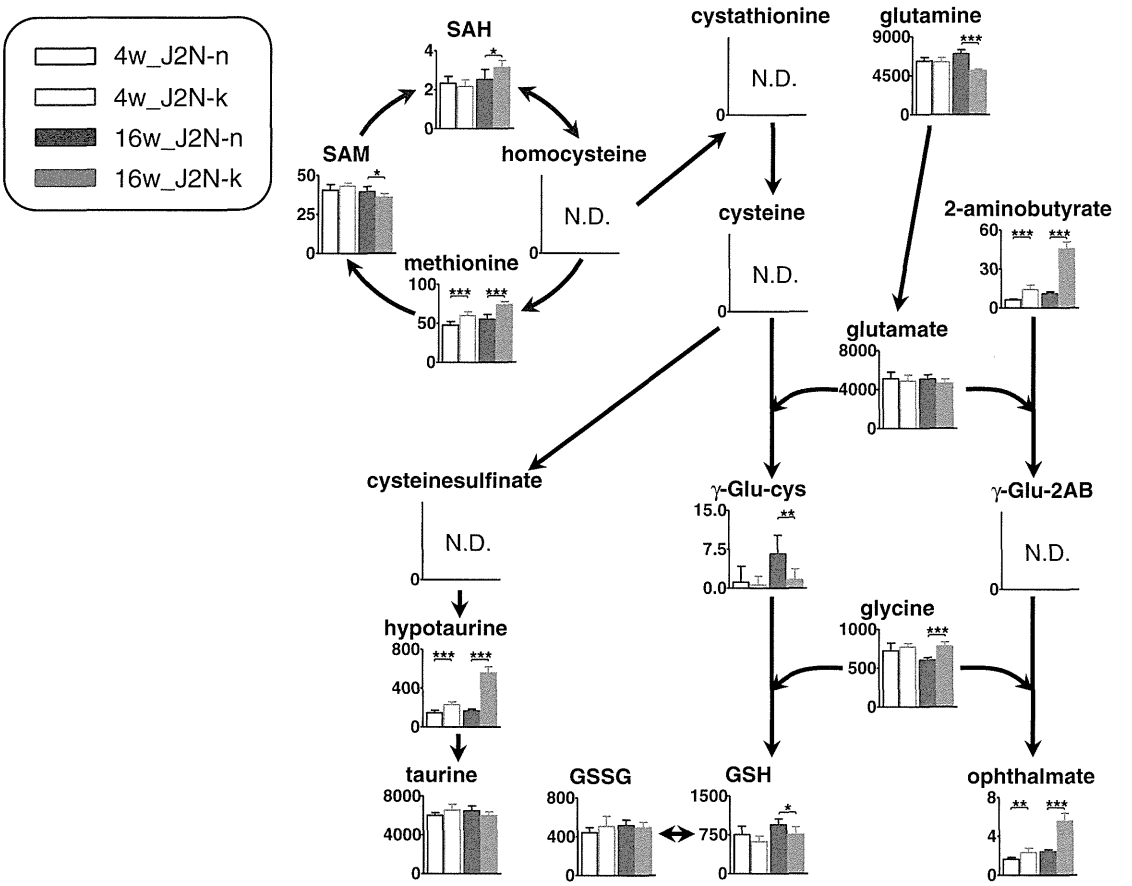

Fig. 3. Quantification of metabolites involved in GSH biosynthesis and related pathways. The columns represent average concentrations (nmol/g tissue), and the error bars indicate SD. *$p<0.05$; **$p<0.01$; ***$p<0.001$; and N.D., not detected.

such as 18:1/18:2PE (0.7-fold, $p=1.5\times10^{-3}$), and 18:0p/20:5PE (0.4-fold, $p=1.0\times10^{-5}$), were markedly reduced in J2N-k tissues at 16 weeks. Thus, the levels of PC and PE species commonly containing linoleic acid (18:2) or EPA (20:5) were reduced at the onset of DCM.

Marked differences between the SM levels and their Cer metabolites were observed in the 2 hamster strains at 16 weeks. For example, the levels of 34:1SM (d18:1/16:0; 1.4-fold, $p=5.1\times10^{-4}$) and 34:1Cer (1.4-fold, $p=4.9\times10^{-2}$) increased, but those of 38:1SM (d18:1/20:0; 0.7-fold, $p=3.3\times10^{-3}$) and 38:1Cer (0.6-fold, $p=3.1\times10^{-3}$) decreased in J2N-k tissue as compared to J2N-n tissue.

The levels of major TAG species significantly decreased in J2N-k compared with J2N-n tissues at 16 weeks (Fig. 5, Supplementary Table 3). Although we could not determine the individual fatty acid chain compositions, many of these species were dramatically decreased, including 54:5TAG (0.5-fold, $p=6.0\times10^{-3}$) and 54:6TAG (0.5-fold, $p=5.4\times10^{-3}$). Furthermore, the levels of 9 DAG species

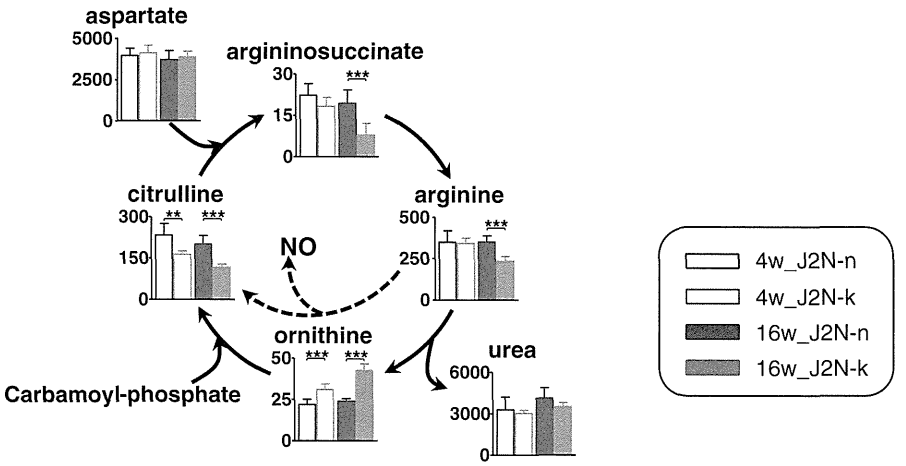

Fig. 4. Metabolic changes in urea cycle metabolism. The dashed lines indicate the NO synthesis pathway, columns represent average concentrations (nmol/g tissue), and error bars indicate SD. *$p<0.05$; **$p<0.01$; and ***$p<0.001$.

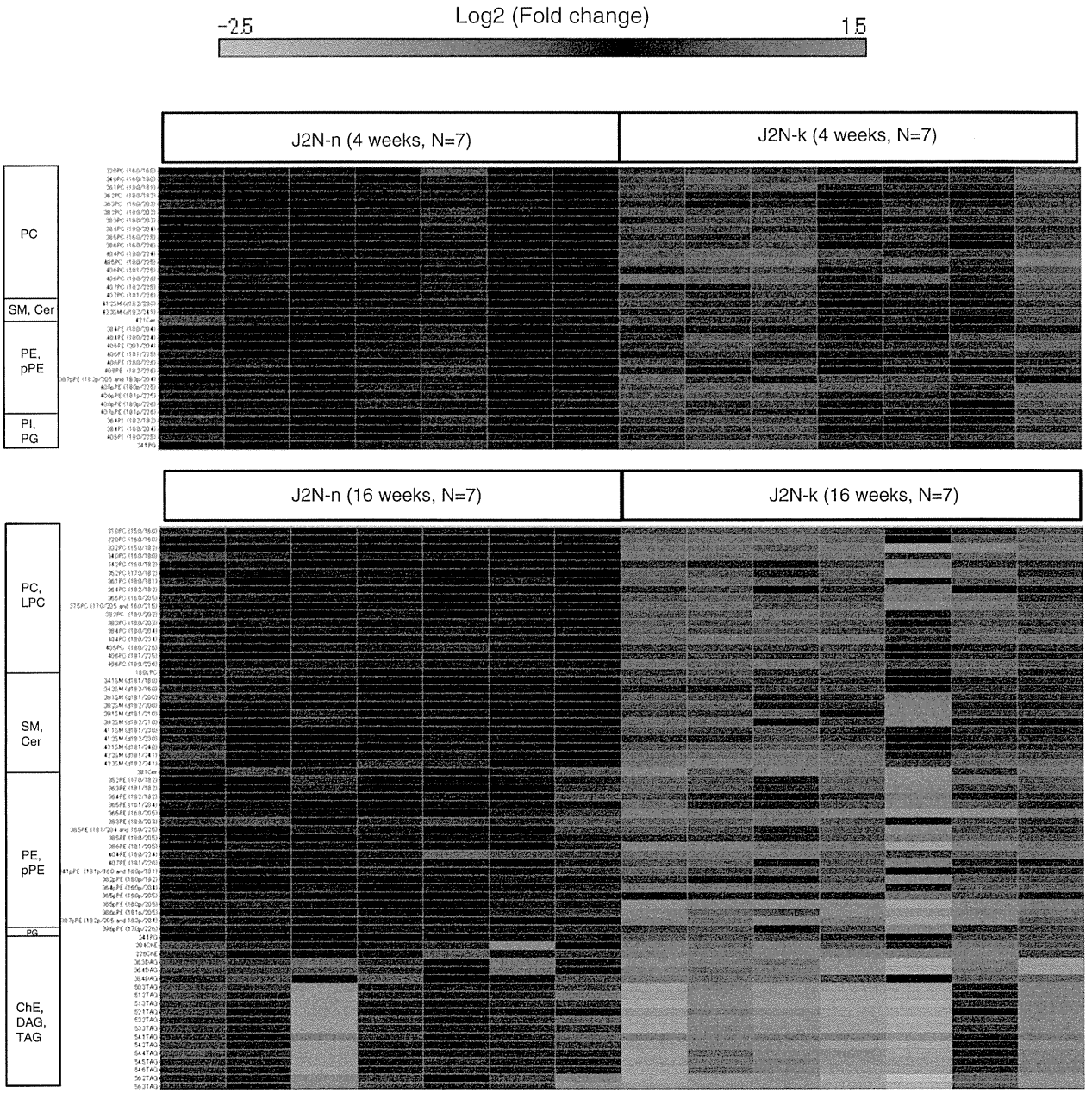

Fig. 5. Heatmap showing relative quantification of lipid metabolites identified in myocardial tissue from J2N-n and J2N-k hamsters ($n=7$ in all groups). Thirty-four (at 4 weeks) and sixty-eight (at 16 weeks) lipid metabolites with different levels ($p<0.01$) in J2N-n and age-matched J2N-k at each time point are shown. Data are represented by the log2 ratio of relative amounts of each metabolite in J2N-k to the mean relative amounts in J2N-n at either 4 or 16 weeks.

changed in J2N-k tissues at 16 weeks: 2 species, including 38:4DAG (1.6-fold, $p=2.4\times10^{-3}$), were increased, while another 7 species, predicted to contain mono- or di-unsaturated fatty acids such as 36:3DAG (0.4-fold, $p=2.2\times10^{-3}$), were significantly decreased.

3.8. Oxidative fatty acids levels were altered in J2N-k myocardial tissues

The levels of 3 prostaglandin (PGs)—PGE_2 (5.1-fold, $p=1.5\times10^{-2}$), PGD_2 (7.8-fold, $p=1.5\times10^{-2}$), and 6-keto-$PGF_{1\alpha}$ (stable metabolite of PGI_2; 8.1-fold, $p=4.6\times10^{-3}$)—were significantly increased in J2N-k myocardial tissue at 16 weeks, compared with J2N-n tissue (Fig. 6, Supplementary Table 4). Moreover, the levels of 12S-hydroxy-5Z; 8E; and 10E-heptadecatrienoic acid (12-HHT), a product of arachidonic acid via the cyclooxygenase pathway, were also increased (5.7-fold, $p=4.7\times10^{-2}$) in these tissues. In addition, levels of cyclooxygenase 2, an enzyme that catalyzes the rate-limiting step of these 4 metabolites, increased at 16 weeks in J2N-k tissue (Supplementary Fig. 7).

3.9. Increased oxidative stress in the DCM heart

Since previous reports, as well as our results (increase in ophthalmate levels), suggest the high oxidative stress levels at 16 weeks of J2N-k hamsters, we assessed lipid peroxidation and superoxide production by 4-HNE staining and DHE staining, respectively (Supplementary Figs. 8 and 9). Results from both staining confirmed an increased oxidative stress in the cardiac tissue of 16-week-old J2N-k hamsters.

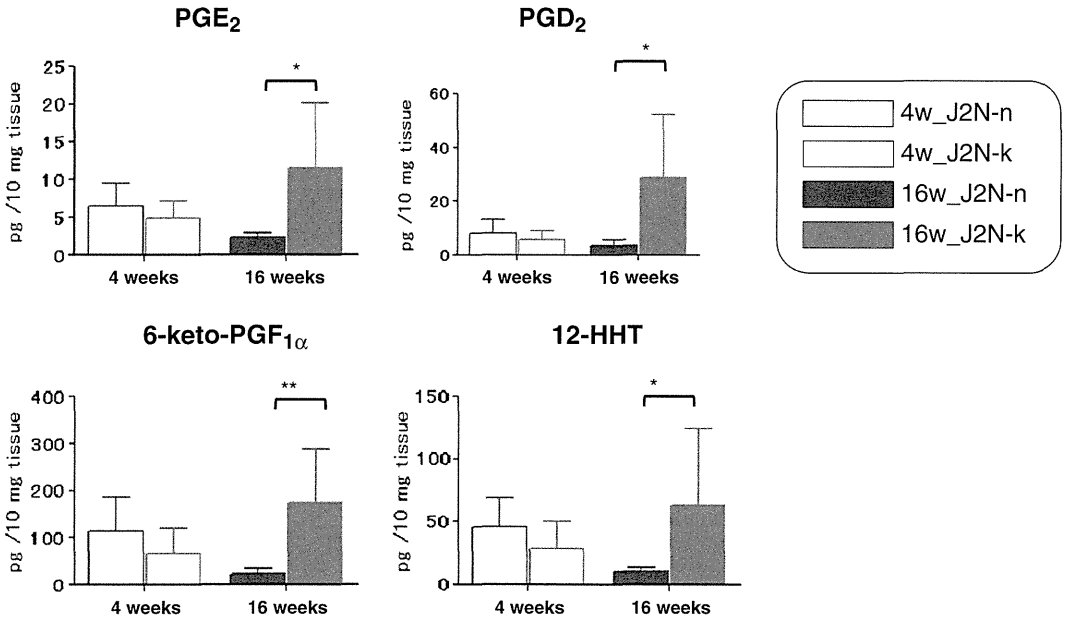

Fig. 6. Levels of 4 eicosanoids in the left ventricular tissues of 4- and 16-week-old J2N-k and J2N-n hamsters. The error bars represent mean ± SD values ($n=7$). *$p<0.05$, **$p<0.01$, and *$p<0.001$.

4. Discussion

We performed global metabolomic analysis on myocardial tissues from J2N-k cardiomyopathic hamsters, which were found to have significantly different profiles of charged and lipid metabolites from those of J2N-n normal controls. In general, mild edema could be seen in the heart with DCM, and cardiomyocyte protein concentrations in 16-week-old J2N-k hamsters (but not 4-week-old hamsters) decreased by 9.5% compared with the J2N-n line at the same age (data not shown). However, this difference did not have a large impact on the variation in metabolite levels between J2N-k and J2N-n hamsters, and the metabolomic results were shown per tissue weights.

Analysis of charged metabolites showed significant reductions in the levels of glycolysis and TCA cycle metabolites in J2N-k myocardial tissues as compared with those of J2N-n at 16 weeks (symptomatic phase; Fig. 2). In addition to these pathways, the creatine kinase pathway also supplies energy to the heart and maintains ATP levels by the rapid transfer of high-energy phosphoryl groups from phosphocreatine to ADP. Creatine and creatinine (degradation products of phosphocreatine) levels in J2N-k symptomatic phase tissues were significantly lower than those in age-matched controls (Supplementary Table 2). It has been reported that creatine levels are attenuated in heart tissue from dystrophin-deficient *mdx* mice [19] and that creatine levels reflect the severity of heart failure in patients with DCM [20]. In addition, carnitine levels are also significantly decreased in J2N-k tissues at 16 weeks (Supplementary Table 2). Since carnitines are used for transporting fatty acids from the cytosol into the mitochondria, the availability of fatty acids for β-oxidation may be reduced in J2N-k hamsters. This supports our finding that acetyl CoA levels are considerably decreased in J2N-k tissue (ratio of 0.3 at 16 weeks, Supplementary Table 2). A recent paper also reported that Bio-TO2 cardiomyopathic hamster hearts showed reduced activity of pyruvate dehydrogenase [21], which catalyzes acetyl CoA production. These findings suggest that decreased energy production occurs in DCM hearts, resulting in reduced cardiac pumping. Further studies, such as flux analysis, are needed to validate these assumptions.

A mild reduction in GSH levels and a considerable loss of its precursor, γ-Glu-Cys in the glutathione biosynthesis pathway, were observed in J2N-k tissues at 16 weeks. In contrast, mild increases at 4 weeks and considerable increases at 16 weeks were observed for levels of ophthalmate and its precursor, 2-AB in J2N-k tissue (Fig. 3). Ophthalmate is synthesized by the same enzymes as those for GSH, but it contains 2-AB instead of cysteine [10]. Although the cysteine levels in myocardial tissue extracts were below the detection limit, the GSH synthesis pathway appeared to be upregulated based on the increased levels of its components methionine and SAH. Instead of cysteine, our data suggests that the upregulated GSH synthesis pathway uses 2-AB for ophthalmate production. This is supported by changes in the levels of other GSH and ophthalmate synthesis components: glycine levels significantly increased and glutamine (a glutamate precursor) levels decreased. We also observed increased levels of hypotaurine at both 4 and 16 weeks (Fig. 3). Unlike taurine, hypotaurine has antioxidant activity that effectively scavenges hydroxyl radicals and hypochlorous acid moieties [22]. These findings suggest that metabolic changes are initiated to counteract the increased oxidative stress observed in DCM heart tissues as confirmed in Supplementary Figs. 8 and 9.

Significant decreases in the urea cycle metabolites, arginine, argininosuccinate, and citrulline, were observed in myocardial tissues of 16-week-old J2N-k hamsters as compared to J2N-n hamsters (Fig. 4). Reductions in arginine and citrulline levels suggest a reduction in nitric oxide (NO) production by nitric oxide synthase. This is consistent with the report that NO concentrations in coronary circulation were lower in DCM patients as compared to control human subjects [23]. In contrast, increased conversion of arginine to ornithine suggests that the high arginase activity in 16-week-old J2N-k hamsters can modulate NO synthesis by limiting arginine availability for NO synthesis. NO is critical for coupling cardiac excitation-contraction by modulating Ca^{2+} homeostasis [24], suggesting its possible relation to DCM.

A recent study found that changes in lipid homeostasis contribute to the development of various cardiomyopathies [25]. In particular, dysregulation of membrane phospholipid homeostasis alters the interaction of membrane-associated protein complexes that modulate cell signaling and myocardial metabolism [26]. At the presymptomatic phase (4 weeks), we observed increased levels of PC containing unsaturated

(especially polyunsaturated) fatty acids and PE/pPE with 22:5 or 22:6 in J2N-k myocardial tissues (Fig. 5; Supplementary Table 3). In the symptomatic phase, significant decreases in PC containing linoleic acid (18:2) and many PE and pPE species, especially those containing 18:2 and/or EPA (20: 5), were observed in J2N-k hamsters. A significant accumulation of ethanolamine phosphate (1.5-fold, $p = 8.7 \times 10^{-6}$) in J2N-k tissues (Supplemental Table 2 and Fig. 1) suggests that function of the PE biosynthetic enzyme, ethanolaminephosphotransferase, may be impaired in the symptomatic phase tissues. Altered levels of the PC and PE species suggest that membrane perturbations, such as fluidity, are probably important for DCM pathology. Consistent with our results, linoleic acid (18:2) content in PC was reported to be significantly decreased in the myocardium of cardiomyopathic BIO 14.6 hamsters during the development of congestive heart failure [27]. Increased PC content (observed at 4 weeks in this study) was reported to inhibit Ca^{2+}-ATPase (SERCA) activity [28], which was indeed decreased in J2N-k cardiomyopathic hamsters [29]. Our data also show that some LPC species were significantly increased at the DCM symptomatic phase. LPCs increase the intracellular calcium concentration $[Ca^{2+}]_i$ by modulating the activities of the cardiac sarcolemmal membrane ion transporters such as SERCA [30], which may compensate for decreased contractile function. These findings suggest that contractile dysfunction in J2N-k myocardial tissue is partly attributable to aberrant PL metabolism.

At 16 weeks, J2N-k myocardial tissues exhibited altered levels of SMs and Cers of various acyl chain lengths (C16–C24; Fig. 5, Supplementary Table 3), suggesting that specific Cer signaling pathways are activated in DCM. For example, levels of Cer containing palmitic acid (16:0), such as 34:1Cer, were augmented in J2N-k tissue at 16 weeks. As 34:1Cer is a major Cer species and is known to be elevated during apoptosis induced by various agents [31]; it is possible that the apoptosis pathway is triggered in the symptomatic phase. The activation of the apoptotic pathway was reported in proteomic analysis of a phospholamban-mutated DCM mouse model [32].

The PCA of TAGs and ChEs revealed only a modest discrimination between J2N-k and J2N-n tissues both at 4 and 16 weeks (Supplementary Fig. 6B), suggesting wide within-group variations. Nevertheless, remarkable reductions were observed in several major TAG species in J2N-k tissues at 16 weeks (Fig. 5, Supplementary Table 3). TAG is stored in cytosolic lipid droplets within cardiomyocytes and ensures a continuous fatty acid supply for mitochondrial oxidation [33]. Therefore, TAG reductions suggest that heart tissue cannot secure enough energy from fatty acid oxidation, thereby leading to impaired function. Consistent with our observations, fatty acid utilization and oxidation were found to be lower in patients with idiopathic DCM than in normal controls [34]. In addition, DAGs (such as 34:2DAG and 36:3DAG) producing TAGs by diacylglycerol acyltransferase were also significantly decreased at 16 weeks (Supplementary Table 3). We observed decreased levels of glycerol-3-phosphate (a precursor of DAG and TAG, Supplementary Table 2) in J2N-k at 16 weeks, which is consistent with our lipid metabolite data.

The eicosanoids, PGE_2, PGD_2, 6-keto-$PGF_{1\alpha}$, and 12-HHT, produced by the COX pathway, were significantly (more than 5-fold) increased in J2N-k tissues at 16 weeks (Fig. 6). Although eicosanoids are generally thought to contribute to inflammatory responses associated with myocardial dysfunction, recent studies have showed that they may also have a cardioprotective role. For example, increased PGE_2 production protects the heart from ischemia-reperfusion injury via PGE_2 receptors 3 (EP3) and 4 (EP4) [35,36]. Furthermore, mice with cardiac-specific EP4 knockout display a DCM-like phenotype [37]. Elevated PGE_2 production may therefore counteract DCM pathophysiology in J2N-k hamsters. In the DCM transgenic mouse model (Tgalphaq*44 mice overexpressing the activated Galphaq protein), elevated levels of PGI_2, the active precursor of 6-keto-$PGF_{1\alpha}$, compensated for reduced NO-dependent coronary vasodilatation due to endothelial dysfunction during late-stage heart failure [38]. PGI_2 also exerted protective effects on cardiomyocytes during cardiac ischemia-reperfusion injury [39]. Elevation of at least some of these 4 eicosanoids may therefore counteract DCM pathophysiology in the J2N-k model.

5. Conclusions

We performed global metabolomic analysis on left ventricular heart tissues from hamsters with hereditary DCM. In the symptomatic phase, the levels of the most significantly altered charged metabolites are mapped to energy metabolism, the glutathione biosynthesis pathway, and the urea cycle. Specifically, a mild reduction in GSH and a compensatory increase in ophthalmate suggested that increased oxidative stress played a role in DCM pathogenesis; this was later confirmed by 4-HNE and DHE histochemistry. Regarding lipid metabolites, disturbances in membrane phospholipid homeostasis (changes in PC and PE species levels) began even at the presymptomatic phase. The potential involvement of specific eicosanoids in the cardioprotective pathways was suggested by increased levels of these metabolites during the symptomatic phase. Further investigation is required to determine how changes in the concentration of the metabolites identified in this study contribute to cardiac dysfunction in DCM. However, our work does provide insight into the mechanisms involved in DCM pathogenesis and may lead to the identification of new targets for therapeutic intervention or diagnosis.

Abbreviations

2-AB	2-aminobutyrate
4-HNE	4-hydroxynonenal
CE	capillary electrophoresis
Cer	ceramide
ChE	cholesterol ester
DAG	diacylglycerols
DCM	dilated cardiomyopathy
DGC	dystrophin-glycoprotein complex
DHA	docosahexaenoic acid
DHE	dihydroethidium,
EPA	eicosapentaenoic acid
GSH	glutathione
HHT	heptadecatrienoic acid
IS	internal standard
LC	liquid chromatography
LPC	lysoPC
MS	mass spectrometry
NO	nitric oxide
PC	phosphatidylcholine
PCA	principal component analysis
PE	phosphatidylethanolamine
PG	prostaglandin;
PL	phospholipid
pPE	plasmalogen PE
RT	retention time
SM	sphingomyelin
TAG	triacylglycerol
TCA	tricarboxylic acid
TOF	time-of-flight

Supplementary data to this article can be found online at http://dx.doi.org/10.1016/j.yjmcc.2013.02.008.

Funding

This work was supported by the Advanced Research for Products Mining Programme [grant number 10-45] from the National Institute of Biomedical Innovation of Japan to NM, TS, and YS.

Disclosures

None.

References

[1] Luk A, Ahn E, Soor GS, Butany J. Dilated cardiomyopathy: a review. J Clin Pathol 2009;62:219–25.
[2] Tigen K, Cevik C. Beta-blockers in the treatment of dilated cardiomyopathy: which is the best? Curr Pharm Des 2010;16:2866–71.
[3] Takeda N. Cardiomyopathy: molecular and immunological aspects (review). Int J Mol Med 2003;11:13–6.
[4] Seidman JG, Seidman C. The genetic basis for cardiomyopathy: from mutation identification to mechanistic paradigms. Cell 2001;104:557–67.
[5] Campbell KP. Three muscular dystrophies: loss of cytoskeleton-extracellular matrix linkage. Cell 1995;80:675–9.
[6] Yucel D, Aydogdu S, Senes M, Topkaya BC, Nebioglu S. Evidence of increased oxidative stress by simple measurements in patients with dilated cardiomyopathy. Scand J Clin Lab Invest 2002;62:463–8.
[7] Demirbag R, Yilmaz R, Erel O, Gultekin U, Asci D, Elbasan Z. The relationship between potency of oxidative stress and severity of dilated cardiomyopathy. Can J Cardiol 2005;21:851–5.
[8] Baumer AT, Flesch M, Wang X, Shen Q, Feuerstein GZ, Bohm M. Antioxidative enzymes in human hearts with idiopathic dilated cardiomyopathy. J Mol Cell Cardiol 2000;32:121–30.
[9] Mitsuhashi S, Saito N, Watano K, Igarashi K, Tagami S, Shima H, et al. Defect of delta-sarcoglycan gene is responsible for development of dilated cardiomyopathy of a novel hamster strain, J2N-k: calcineurin/PP2B activity in the heart of J2N-k hamster. J Biochem 2003;134:269–76.
[10] Soga T, Baran R, Suematsu M, Ueno Y, Ikeda S, Sakurakawa T, et al. Differential metabolomics reveals ophthalmic acid as an oxidative stress biomarker indicating hepatic glutathione consumption. J Biol Chem 2006;281:16768–76.
[11] Nakamura K, Kusano K, Nakamura Y, Kakishita M, Ohta K, Nagase S, et al. Carvedilol decreases elevated oxidative stress in human failing myocardium. Circulation 2002;105:2867–71.
[12] Fujii T, Onohara N, Maruyama Y, Tanabe S, Kobayashi H, Fukutomi M, et al. Galpha12/13-mediated production of reactive oxygen species is critical for angiotensin receptor-induced NFAT activation in cardiac fibroblasts. J Biol Chem 2005;280:23041–7.
[13] Soga T, Igarashi K, Ito C, Mizobuchi K, Zimmermann HP, Tomita M. Metabolomic profiling of anionic metabolites by capillary electrophoresis mass spectrometry. Anal Chem 2009;81:6165–74.
[14] Soga T, Heiger DN. Amino acid analysis by capillary electrophoresis electrospray ionization mass spectrometry. Anal Chem 2000;72:1236–41.
[15] Bligh EG, Dyer WJ. A rapid method of total lipid extraction and purification. Can J Biochem Physiol 1959;37:911–7.
[16] Taguchi R, Ishikawa M. Precise and global identification of phospholipid molecular species by an Orbitrap mass spectrometer and automated search engine Lipid Search. J Chromatogr A 2010;1217:4229–39.
[17] Sugimoto M, Wong DT, Hirayama A, Soga T, Tomita M. Capillary electrophoresis mass spectrometry-based saliva metabolomics identified oral, breast and pancreatic cancer-specific profiles. Metabolomics 2010;6:78–95.
[18] Ono M, Shitashige M, Honda K, Isobe T, Kuwabara H, Matsuzuki H, et al. Label-free quantitative proteomics using large peptide data sets generated by nanoflow liquid chromatography and mass spectrometry. Mol Cell Proteomics 2006;5:1338–47.
[19] Gulston MK, Rubtsov DV, Atherton HJ, Clarke K, Davies KE, Lilley KS, et al. A combined metabolomic and proteomic investigation of the effects of a failure to express dystrophin in the mouse heart. J Proteome Res 2008;7:2069–77.
[20] Nakae I, Mitsunami K, Yoshino T, Yoshino T, Omura T, Tsutamoto T, et al. Clinical features of myocardial triglyceride in different types of cardiomyopathy assessed by proton magnetic resonance spectroscopy: comparison with myocardial creatine. J Card Fail 2010;16:812–22.
[21] Missihoun C, Zisa D, Shabbir A, Lin H, Lee T. Myocardial oxidative stress, osteogenic phenotype, and energy metabolism are differentially involved in the initiation and early progression of delta-sarcoglycan-null cardiomyopathy. Mol Cell Biochem 2009;321:45–52.
[22] Aruoma OI, Halliwell B, Hoey BM, Butler J. The antioxidant action of taurine, hypotaurine and their metabolic precursors. Biochem J 1988;256:251–5.
[23] Takarada S, Imanishi T, Goto M, Mochizuki S, Ikejima H, Tsujioka H, et al. First evaluation of real-time nitric oxide changes in the coronary circulation in patients with non-ischaemic dilated cardiomyopathy using a catheter-type sensor. Eur Heart J 2010;31:2862–70.
[24] Zima AV, Blatter LA. Redox regulation of cardiac calcium channels and transporters. Cardiovasc Res 2006;71:310–21.
[25] Wende AR, Abel ED. Lipotoxicity in the heart. Biochim Biophys Acta 1801;2010: 311–9.
[26] Jenkins CM, Cedars A, Gross RW. Eicosanoid signalling pathways in the heart. Cardiovasc Res 2009;82:240–9.
[27] Okumura K, Yamada Y, Kondo J, Hashimoto H, Ito T, Kitoh J. Decreased 1,2-diacylglycerol levels in myopathic hamster hearts during the development of heart failure. J Mol Cell Cardiol 1991;23:409–16.
[28] Fu S, Yang L, Li P, Hofmann O, Dicker L, Hide W, et al. Aberrant lipid metabolism disrupts calcium homeostasis causing liver endoplasmic reticulum stress in obesity. Nature 2011;473:528–31.
[29] Babick AP, Cantor EJ, Babick JT, Takeda N, Dhalla NS, Netticadan T. Cardiac contractile dysfunction in J2N-k cardiomyopathic hamsters is associated with impaired SR function and regulation. Am J Physiol Cell Physiol 2004;287: C1202–8.
[30] Yu L, Netticadan T, Xu YJ, Panagia V, Dhalla NS. Mechanisms of lysophosphatidylcholine-induced increase in intracellular calcium in rat cardiomyocytes. J Pharmacol Exp Ther 1998;286:1–8.
[31] Pewzner-Jung Y, Ben-Dor S, Futerman AH. When do Lasses (longevity assurance genes) become CerS (ceramide synthases)?: insights into the regulation of ceramide synthesis. J Biol Chem 2006;281:25001–5.
[32] Gramolini AO, Kislinger T, Alikhani-Koopaei R, Fong V, Thompson NJ, Isserlin R, et al. Comparative proteomics profiling of a phospholamban mutant mouse model of dilated cardiomyopathy reveals progressive intracellular stress responses. Mol Cell Proteomics 2008;7:519–33.
[33] Banke NH, Wende AR, Leone TC, O'Donnell JM, Abel ED, Kelly DP, et al. Preferential oxidation of triacylglyceride-derived fatty acids in heart is augmented by the nuclear receptor PPARalpha. Circ Res 2010;107:233–41.
[34] Dávila-Román VG, Vedala G, Herrero P, de las Fuentes L, Rogers JG, Kelly DP, et al. Altered myocardial fatty acid and glucose metabolism in idiopathic dilated cardiomyopathy. J Am Coll Cardiol 2002;40:271–7.
[35] Martin M, Meyer-Kirchrath J, Kaber G, Jacoby C, Flögel U, Schrader J, et al. Cardiospecific overexpression of the prostaglandin EP3 receptor attenuates ischemia-induced myocardial injury. Circulation 2005;112:400–6.
[36] Xiao CY, Yuhki K, Hara A, Fujino T, Kuriyama S, Yamada T, et al. Prostaglandin E2 protects the heart from ischemia-reperfusion injury via its receptor subtype EP4. Circulation 2004;109:2462–8.
[37] Harding P, Yang XP, Yang J, Shesely E, He Q, LaPointe MC. Gene expression profiling of dilated cardiomyopathy in older male EP4 knockout mice. Am J Physiol Heart Circ Physiol 2010;298:H623–32.
[38] Drelicharz L, Kozlovski V, Skorka T, Heinze-Paluchowska S, Jasinski A, Gebska A, et al. NO and PGI(2) in coronary endothelial dysfunction in transgenic mice with dilated cardiomyopathy. Basic Res Cardiol 2008;103:417–30.
[39] Xiao CY, Hara A, Yuhki K, Fujino T, Ma H, Okada Y, et al. Roles of prostaglandin I(2) and thromboxane A(2) in cardiac ischemia-reperfusion injury: a study using mice lacking their respective receptors. Circulation 2001;104:2210–25.

Cardiovascular Research (2013) **99**, 760–768
doi:10.1093/cvr/cvt163

Blockade of sarcolemmal TRPV2 accumulation inhibits progression of dilated cardiomyopathy

Yuko Iwata[1]*, Hitomi Ohtake[1], Osamu Suzuki[2], Junichiro Matsuda[2], Kazuo Komamura[3], and Shigeo Wakabayashi[1]

[1]Department of Molecular Physiology, National Cerebral and Cardiovascular Center Research Institute, Fujishiro-dai 5-7-1, Suita, Osaka 565-8565, Japan; [2]Laboratory of Animal Models for Human Diseases, National Institute of Biomedical Innovation, Ibaraki, Osaka 567-0085, Japan; and [3]Department of Clinical Pharmacology and Pharmacogenomics, Graduate School of Pharmaceutical Science, Osaka University, Suita, Osaka 565-0871, Japan

Received 23 January 2013; revised 1 June 2013; accepted 14 June 2013; online publish-ahead-of-print 19 June 2013

Time for primary review: 10 days

Aims Dilated cardiomyopathy (DCM) is a severe disorder defined by ventricular dilation and contractile dysfunction. Abnormal Ca^{2+} handling is hypothesized to play a critical pathological role in DCM progression. The transient receptor potential vanilloid 2 (TRPV2) has been previously suggested as a candidate pathway for enhanced Ca^{2+} entry. Here, we examined the sarcolemmal accumulation of TRPV2 in various heart-failure model animals and DCM patients, and assessed whether presently available inhibitory tools against TRPV2 ameliorate DCM symptoms.

Methods and results Immunological and cell physiological analyses revealed that TRPV2 is highly concentrated and activated in the ventricular sarcolemma of DCM patients and three animal models—δ-sarcoglycan-deficient hamsters (J2N-k), transgenic mice over-expressing sialytransferase (4C30), and doxorubicin (DOX)-induced DCM mice. Over-expression of the amino-terminal (NT) domain of TRPV2 could block the plasma membrane accumulation and influx of Ca^{2+} via TRPV2. Transgenic (Tg) or adenoviral expression of the NT domain in DCM animals caused effective removal of sarcolemmal TRPV2 along with reduction in the phosphorylation of calmodulin-dependent protein kinase II (CaMKII) and reactive oxygen species (ROS) production, which were activated in DCM; further, it prevented ventricular dilation and fibrosis, ameliorated contractile dysfunction in DCM, and improved survival of the affected animals. The TRPV2 inhibitor tranilast markedly suppressed DCM progression.

Conclusion Sarcolemmal TRPV2 accumulation appears to have considerable pathological impact on DCM progression, and blockade of this channel may be a promising therapeutic strategy for treating advanced heart failure.

Keywords Dilated cardiomyopathy • Heart failure • Therapeutic tool • Ca^{2+}-permeable channel • DOX-induced cardiomyopathy

1. Introduction

Dilated cardiomyopathy (DCM) is a severe disorder defined by ventricular dilation and cardiac dysfunction.[1–3] Although a considerable proportion of DCM cases develop because of inflammatory, metabolic, or toxic effects from medications, 30–48% of DCM cases are caused by genetic mutations.[4] Some affected genes encode sarcomeric or cytoskeletal proteins, including the components of the dystrophin–glycoprotein complex (DGC).[5,6] For example, δ-sarcoglycan-deficient hamsters (J2N-k) provide an animal model of human limb-girdle muscular dystrophy-associated DCM. However, little information is available regarding the pathways by which heterogeneous genetic defects and/or various causes lead to DCM symptoms.

The calcium ion (Ca^{2+}) plays a pivotal role in the pathogenesis of cardiac disease.[7,8] Ca^{2+}-handling abnormalities have been found in various forms of heart failure, including DCM.[9–11]

Further Ca^{2+}-permeable transient receptor potential (TRP) channels have recently been recognized as key molecules in pathological cardiac hypertrophy and heart failure.[12–14] We have previously reported that cardiac-specific over-expression of TRP vanilloid 2 (TRPV2) results in DCM with outstanding ventricular dilation,[15] suggesting that chronic elevation in cytosolic Ca^{2+} concentrations ($[Ca^{2+}]_i$) is critical in DCM pathogenesis. However, it is unclear whether TRPV2 activity is a risk factor for DCM in humans as well as animals and whether TRPV2 inhibition can be beneficial against DCM progression, because of the limited number of methods for specific TRPV2 inhibition.

* Corresponding author. Tel: +81 6833 5012; fax: +81 6 6835 5314, Email: yukoiwat@ri.ncvc.go.jp

Therefore, we examined the role of TRPV2 in DCM. We also assessed the effect of TRPV2 blockades on cardiac dysfunction and DCM progression in several animal models.

2. Methods

Detailed methods are available in the Supplementary material online.

2.1 Molecular biology

All plasmid construction involving TRPV2 was carried out via a PCR-based strategy using the full-length mouse TRPV2 cDNA cloned into the pIRES expression vector (Invitrogen). Restriction enzyme-digested PCR products corresponding to the amino-terminal (NT) (amino acids (aa) 1–387) and carboxyl-terminal (CT) (aa 633–756) domains of TRPV2 were cloned into the p3Xflag-CMV-14 expression vector (Sigma-Aldrich). For adenoviral gene transfer, we inserted the haemagglutinin (HA)-tagged NT domain of TRPV2 (amino acids 1–387) cDNA into the pAd/CMV/V5-DEST viral vector (Invitrogen).

2.2 Animals and drug administration

DCM mice (4C30) were produced as described previously.[16] Heart-specific NT-transgenic (Tg) mice were generated from C57BL/6J mice according to the standard procedures.[15]

J2N-k hamsters, and age-matched normal controls (J2N-n) were purchased from Japan SLC. J2N-k hamsters were orally administered tranilast for 14 days at a dose of 30 or 300 mg/kg per day. In the DOX experiment, wild-type (WT) and NT-Tg mice were chronically treated with either phosphate-buffered saline (PBS; control) or doxorubicin (DOX) (Pfizer) by four intraperitoneal (i.p) injections (d 0, 2, 4, and 6) at a dose of 4 mg/kg (cumulative dose totalling 16 mg/kg). All animal experiments were performed in accordance with the Guidelines for Animal Experimentation of the National Cerebral and Cardiovascular Center (NCVC), and procedures were carried out in accordance with the Guide for the Care and Use of Laboratory Animals published by the US National Institutes of Health (NIH; NIH Publication, 8th Edition, 2011).

2.3 Histology, immunoblotting, and immunohistochemistry

Animals were anaesthetized with 5% isoflurane in an anaesthesia chamber until unresponsive to nose pinch, and the heart was harvested for

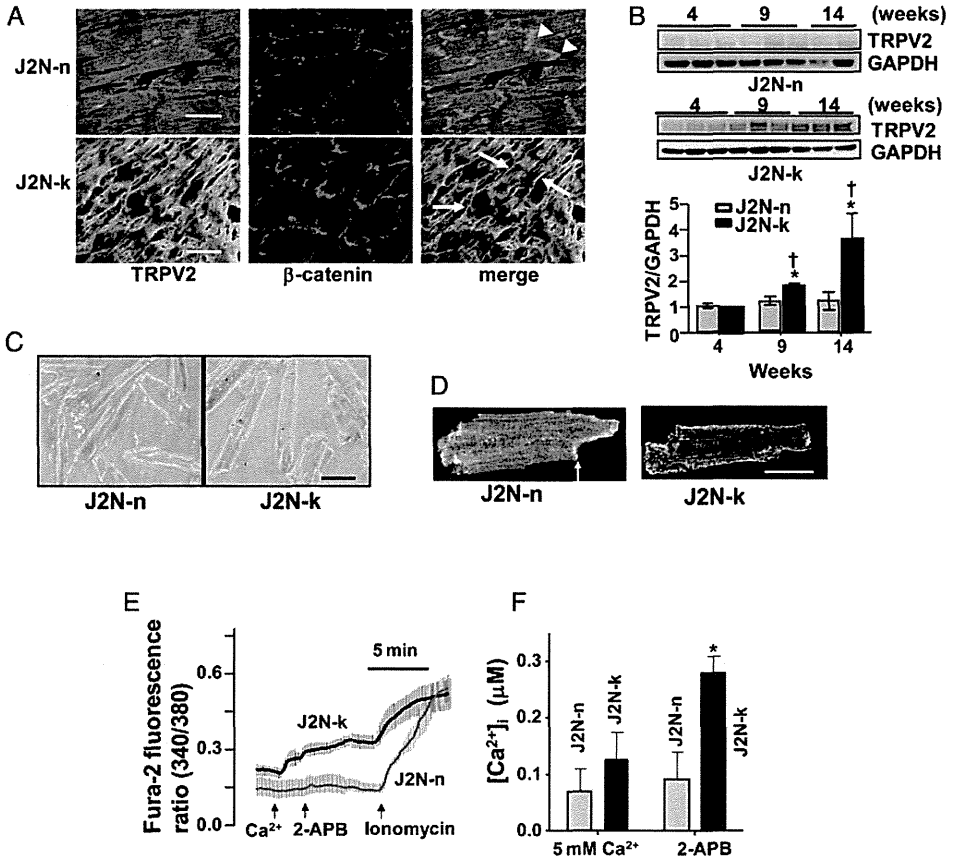

Figure 1 TRPV2 accumulation and activation in the sarcolemma of cardiomyopathic hearts. (*A*) Immunohistochemical analysis of frozen ventricular sections from 8-week-old J2N-n and J2N-k hamsters with TRPV2 and β-catenin antibodies. β-catenin-positive intercalated discs or sarcolemmal regions are shown by arrowheads or arrows, respectively. Scale bar: 50 μm. (*B*) Immunoblots (40 μg/lane) of TRPV2-immunostained cardiac muscles. Age-dependent increases in the expression level of TRPV2 are observed. The data represent mean ± SD values ($n = 4–6$ hamsters/group); $^*P < 0.05$ vs. 4 weeks, $^\dagger P < 0.05$ vs. J2N-n. (*C*) Phase-contrast micrographs of freshly isolated ventricular cardiomyocytes. Scale bar: 30 μm. (*D*) Confocal micrographs of TRPV2-immunostained isolated cardiomyocytes. TRPV2 is extensively localized to the sarcolemma in J2N-k cells but to the intracellular compartment and intercalated disc (arrow) in J2N-n cells. Scale bar: 30 μm. (*E*) Intracellular Ca^{2+} increase in response to extracellular Ca^{2+} (5 mM) and 2-APB (500 μM) in cardiomyocytes loaded with fura-2. (*F*) Intracellular Ca^{2+} concentration calculated from three independent experiments. The data represent mean ± SD values ($n = 7–10$ cardiomyocytes/group); $^*P < 0.05$.

biochemical assays. These experiments were conducted as described previously.[15,17,18]

2.4 Echocardiography

Cardiac function was evaluated by echocardiography using a Hewlett Packard Sonos 5500 ultrasound system with a 12-MHz transducer and M-mode imaging. Animals were sedated with tribromoethanol [i.p, 350 mg/kg of body weight (BW)] during the procedure.

2.5 Cardiomyocyte isolation and $[Ca^{2+}]_i$ measurement

Single-ventricular cardiomyocytes were freshly isolated from adult mouse and hamster hearts using standard enzymatic techniques.[19] The $[Ca^{2+}]_i$ was measured at room temperature via a ratiometric fluorescence method using fura-2 or indo-1 acetoxymethyl ester.[17,19]

2.6 Human tissues

Cardiac tissue samples were obtained from patients with DCM (Supplementary material online, *Table*). Written informed consent was obtained from all living patients, and the experiments on human tissues were approved by the Institutional Review Board of the NCVC. The investigation conforms to the principles of the Declaration of Helsinki.

2.7 Statistical analysis

We used an unpaired Student's *t*-test and one-way ANOVA followed by Dunnett's test for statistical analysis. $P < 0.05$ indicates statistical significance.

3. Results

3.1 TRPV2 is concentrated and activated in cardiomyopathic hearts

To study the role of TRPV2 in DCM, we first examined the expression and subcellular distribution of TRPV2 in the ventricles of δ-sarcoglycan-deficient (J2N-k) hamsters. In their normal control counterparts (J2N-n, 8-week-old hamsters), most of the TRPV2 expression was observed in the cell interior and in regions co-stained with the intercalated disc marker β-catenin (*Figure 1A*). In contrast, age-matched J2N-k ventricles showed increased TRPV2 expression in the peripheral sarcolemma as well as in parts of the intercalated discs (*Figure 1A*). With disease progression, total TRPV2 expression levels gradually increased only in J2N-k ventricles (from 9-week-old hamsters; *Figure 1B*). Although apparently similar rod shapes and sizes were noted in isolated cardiomyocytes from both types of hamsters (*Figure 1C*), stronger TRPV2 surface expression was observed in J2N-k cardiomyocytes than in controls (*Figure 1D*).

In J2N-k cardiomyocytes expressing TRPV2 in the sarcolemma, a rapid and large increase in $[Ca^{2+}]_i$ was elicited by exposure to the TRPV2 channel activator 2-aminoethoxydiphenyl borate (2-APB) as well as a high-Ca^{2+} solution, whereas increases in $[Ca^{2+}]_i$ were marginal in control J2N-n cardiomyocytes (*Figure 1E* and *F*); this increase was inhibited by the TRPV channel antagonist ruthenium red (data not shown). Although TRPV1–3 are known to be activated by 2-APB,[20] cardiac tissues did not show detectable TRPV1 or TRPV3 expression (data not shown). Furthermore, although 2-APB is known to inhibit the intracellular Ca^{2+}-release channel inositol 1, 4, 5-trisphosphate receptor (IP_3R) and other TRP channel family proteins,[21] we saw an

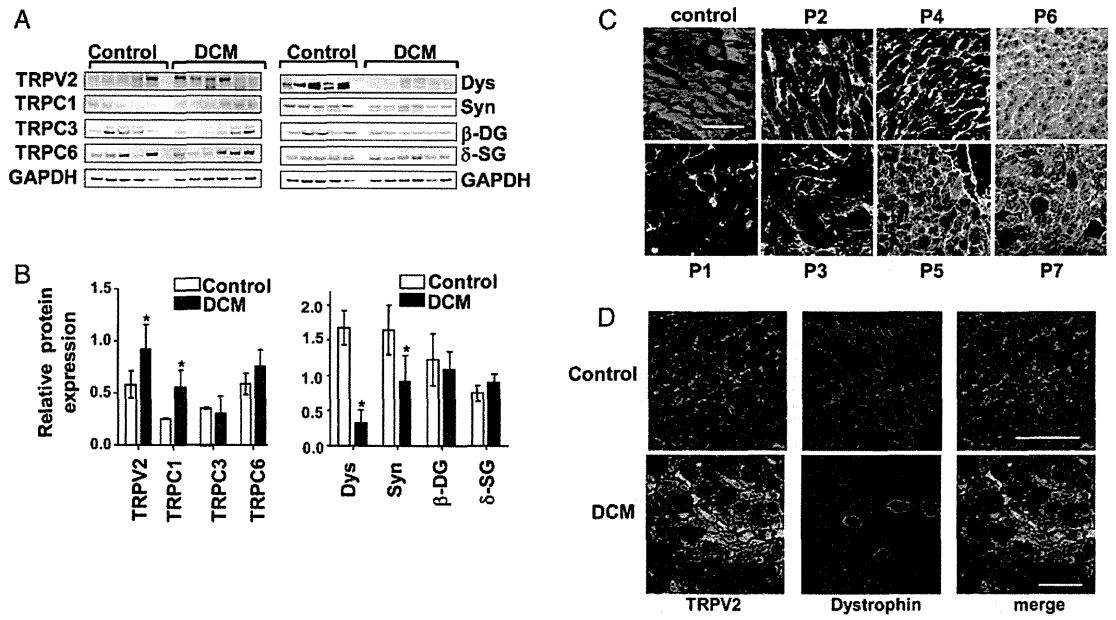

Figure 2 Sarcolemmal TRPV2 accumulation in human DCM. (*A*) Representative immunoblot data of human heart homogenates. Controls and DCM patients; dys, dystrophin; syn, syntrophin; DG, dystroglycan; SG, sarcoglycan; TRPC, transient receptor potential canonical. (*B*) Protein expression levels relative to GAPDH expression in control (white bars) and patient (black bars) samples. The data represent mean ± SD values from four4 independent experiments ($n = 5–7$ samples/group); $^*P < 0.05$. (*C*) TRPV2 immunostaining of frozen human ventricular sections. P1–P7 (Supplementary material online, *Table S1*). Scale bar: 100 μm. (*D*) Ventricular sections from control and DCM patient were co-immunostained with TRPV2 and dystrophin. Note the surface localizsation of TRPV2 and reduced number of dystrophin-positive myocytes in DCM. Scale bar: 100 μm.

increase in $[Ca^{2+}]_i$, which is why TRPV2 was considered the principal candidate involved in the 2-APB-induced $[Ca^{2+}]_i$ increase in J2N-k cardiomyocytes. In addition, we observed that 2-APB often induced abnormal Ca^{2+} elevation accompanied by loss of regular Ca^{2+}-transients under electrically stimulated conditions in J2N-k cardiomyocytes (but not in J2N-n control cardiomyocytes; unpublished observations). These data suggest that sarcolemmal TRPV2 accumulation contributes to the increased $[Ca^{2+}]_i$ levels in J2N-k cardiomyocytes.

In addition to the J2N-k hamster, other animal models with DCM display sarcolemmal accumulation of TRPV2. One such model is the 4C30 mouse, which over-expresses β-galactoside α-2,3-sialytransferase II (ST3Gal-II) and was recently developed as a model for human DCM; the other is DOX-induced DCM, a widely familiar model, although its precise mechanism of cardiotoxicity remains debatable. In hearts from these two animal models, total expression (see *Figures 4A* and *5E*) and sarcolemmal accumulation of TRPV2 (see *Figures 4B* and *5D* and Supplementary material online, *Figures S1* and *S2*) were found to be largely increased when compared with WT mice. In 4C30 mice, expression of TRP canonical (TRPC6), but not that of TRPC1 and TRPC3, was slightly increased (Supplementary material online, *Figure S3*); however, expression of α-dystroglycan and α-sarcoglycan were greatly reduced (Supplementary material online, *Figure S4*).

We next studied TRPV2 expression in ventricular samples from DCM patients (Supplementary material online, *Table S1*). TRPV2 and TRPC1 expression was significantly higher in DCM patients than in controls (*Figure 2A* and *B*), but expression of TRPC3 and TRPC6 was not significantly different. All DCM samples also exhibited reduced dystrophin and syntrophin expression levels (*Figure 2A* and *B*), suggesting that DCM is somehow linked to abnormal cytoskeletal organization. Similar to the findings in J2N-k ventricles, strong TRPV2 immunostaining was detected only in the peripheral sarcolemma of DCM cardiomyocytes (*Figure 2C*). Part of the TRPV2 expression was co-localized with the subsarcolemmal cytoskeletal protein dystrophin in human DCM ventricles, although dystrophin was detected only in a limited number of myocytes (*Figure 2D*).

3.2 Over-expression of the NT domain effectively blocks plasma membrane accumulation of TRPV2

We hypothesized that sarcolemmal TRPV2 accumulation is a common factor leading to Ca^{2+}-induced muscle degeneration in various heart diseases. Therefore, translocation of TRPV2 from the sarcolemma to the cell interior could be a promising therapeutic method. To study such 'back-translocation' of TRPV2, we used HEK293 cells, because they always recruit TRPV2 to the plasma membrane, independent of growth conditions, upon its heterologous expression (*Figure 3A*). We examined over-expression of several functional domains of TRPV2 together with full-length TRPV2 to identify the part of the TRPV2 molecule required for plasma membrane accumulation. We found that when the NT domain of TRPV2 was over-expressed, the majority of TRPV2 molecules moved from the sarcolemma to the cell interior (*Figure 3A*); such translocation was not observed with CT domain over-expression (*Figure 3A*). Consistent with this, over-expression of the NT but not the CT domain dramatically inhibited 2-APB-induced $[Ca^{2+}]_i$ increase (*Figure 3B* and *C*). Thus, the NT domain may be a useful tool for abrogating the sarcolemmal TRPV2 accumulation, thereby inhibiting the sustained increase in $[Ca^{2+}]_i$ in agonist-stimulated cells. To examine the effect of NT domain over-expression on DCM symptoms, we used 4C30 mice and DOX-induced DCM mice.

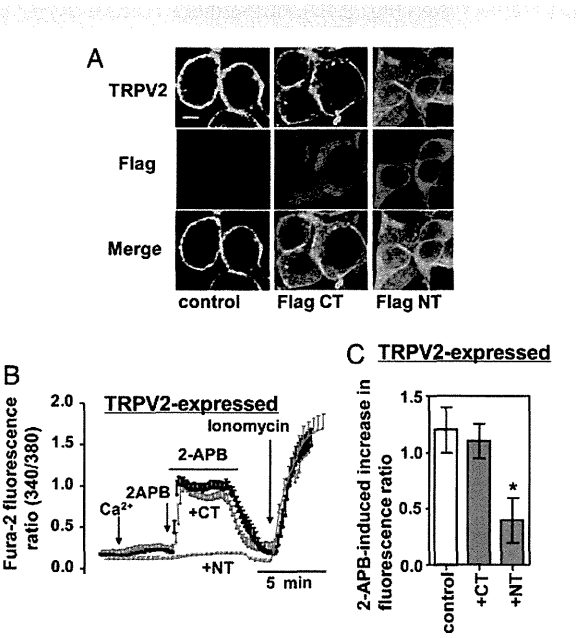

Figure 3 Over-expression of the TRPV2 NT domain blocks the surface expression of TRPV2. (*A*) HEK293 cells expressing TRPV2 were transfected with Flag-tagged CT or NT domain and immunostained with anti-TRPV2 and anti-Flag antibodies. Note that the over-expression of the NT domain reduced TRPV2 surface expression. Scale bar: 10 μm. (*B*) Intracellular Ca^{2+} increase in response to extracellular Ca^{2+} (5 mM) and 2-APB (500 μM) in cells loaded with fura-2. (*C*) The peak fura-2 ratio induced by 2-APB was summarized from three independent experiments. The data represent mean ± SD values (n = over 10 cells/group); $^*P < 0.05$.

3.3 Tg expression of the NT domain ameliorates cardiomyopathy in 4C30 mice

We generated Tg mice expressing the HA-tagged NT domain (*Figure 4A*) under the control of the α-myosin heavy chain (α-MHC) promoter. NT-Tg mice were apparently healthy as evidenced by normal heart morphology (*Figure 4C*), cardiac function (*Figure 4G* and *H*) and life span (*Figure 4I*). The NT domain was introduced into the hearts of 4C30 mice by crossing them with NT-Tg mice. Interestingly, elevated expression level of endogenous TRPV2 in 4C30 mice was decreased to control levels in 4C30/NT-Tg mice (*Figure 4A*). The exogenous NT domain was mostly localized to intercalated discs in both NT-Tg and 4C30/NT-Tg mice (*Figure 4B*). As expected, the sarcolemmal localization of TRPV2 in 4C30 mice was dramatically reduced following NT domain over-expression (4C30/NT-Tg) (*Figure 4B*), potentially leading to a reduction in sustained $[Ca^{2+}]_i$ increase. Consistent with this idea, CaMKII phosphorylation was markedly reduced in the 4C30/NT-Tg mice (*Figure 4A*). In addition, the expression level of modulatory calcineurin inhibitory protein-1 (MCIP) was increased in 4C30 mice but reduced in 4C30/NT-Tg mice (*Figure 4A*), further suggesting that blockade of TRPV2 results in a reduction in sustained $[Ca^{2+}]_i$ increase.

In 4C30 mice aged more than 120 days, we observed thinner ventricular walls and greater ventricular dilation accompanied by fibrosis (*Figure 4C*), with increased serum cardiac troponin I (cTnI; a heart

injury marker) levels (*Figure 4D*). Furthermore, reactive oxygen species (ROS) production measured by dihydroethidium (DHE) staining (*Figure 4E*) and the extent of lipid peroxidation estimated by measurement of 4-hydroxynonenal (4-HNE) adducts (*Figure 4F*) were significantly higher in the 4C30 mice, suggesting high oxidative stress in these DCM hearts. The 4C30/NT-Tg mice showed marked suppression of these symptoms (*Figure 4C–F*). Echocardiographically, the 4C30 mice showed increased left-ventricular diastolic and systolic dimensions (LVDd and LVDs, respectively), with decreased fractional shortening (FS) and ejection fractions (EF) (*Figure 4G* and *H*). However, the 4C30/NT-Tg mice had significantly improved cardiac functions. Moreover, the 4C30 mice progressively died at 200–300 days after birth, but 4C30/NT-Tg mice had a much longer life span, particularly the female mice (*Figure 4I*). We suspect that the amelioration in DCM symptoms may have resulted from the removal of endogenous TRPV2 from the sarcolemma.

3.4 Beneficial effects of NT domain over-expression in DOX-induced DCM

The effects of NT domain over-expression were next examined in DOX-induced DCM. In WT mice, DOX treatment resulted in ventricular dilation, reduced FS, and higher mortality (*Figure 5A–C*). In contrast, DOX-treated NT-Tg mice demonstrated better cardiac morphology and function and better survival (*Figure 5A–C*). Indeed, upon DOX treatment, the NT-Tg mice showed lower TRPV2 expression and sarcolemmal accumulation of TRPV2 (*Figure 5D* and *E*), demonstrating reduced CaMKII phosphorylation (*Figure 5E*) and oxidative stress (*Figure 5F* and *G*). These results suggest that TRPV2 also plays an important pathological role in non-genetic heart failure, such as DOX-induced DCM.

3.5 Adenoviral expression of the NT domain ameliorates cardiac dysfunction in J2N-k hamsters

We next addressed whether the effects of the NT domain could be seen in J2N-k cardiomyopathy following over-expression via adenoviral transfer. We injected an adenovirus carrying either β-galactosidase (β-gal; as a control) or the NT domain into the hearts of 9-week-old J2N-k hamsters, at which age sarcolemmal TRPV2 translocation and cardiac dysfunction had already been observed. At 14 days post-injection, we detected NT domain expression in the ventricles by immunoblotting with the HA antibody (*Figure 6A*). Detection of green fluorescent protein (GFP) in cardiac homogenates (*Figure 6A*) and sections (*Figure 6B*) confirmed that the adenoviral vector had reached the

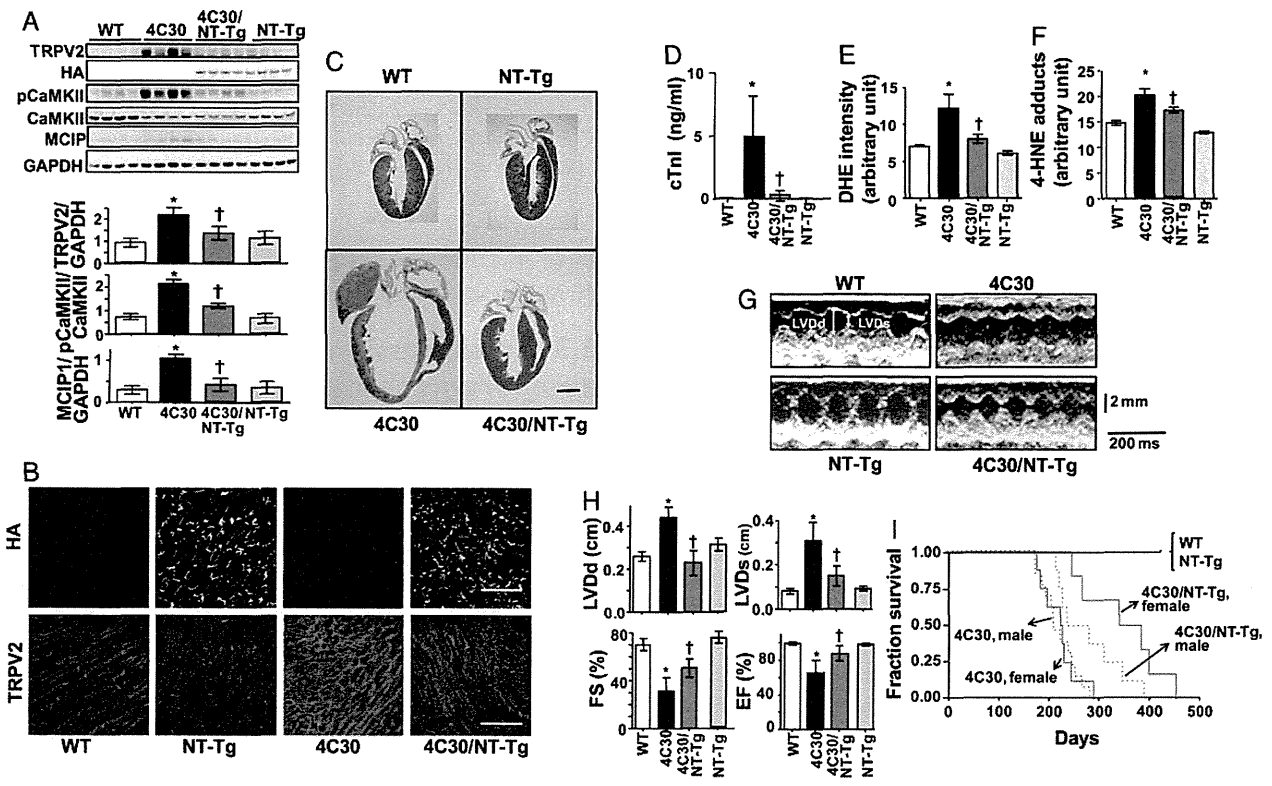

Figure 4 Over-expression of the NT domain blocks TRPV2 surface expression and ameliorates morphological and biochemical symptoms of cardiomyopathy in 4C30 mice. (*A*) Representative immunoblot of heart homogenates with the indicated antibodies (upper panel). Data represent values from four independent experiments ($n = 3–4$/group) $^{*}P < 0.05$ vs. WT mice, $^{\dagger}P < 0.05$ vs. 4C30 mice. (*B*) Representative immunohistochemical data from longitudinal cardiac sections from each group of mice. Scale bar: 100 μm. (*C*) Cardiac sections from 150-day-old mice stained with Masson's trichrome. Scale bar: 5 mm. (*D*) Level of cTnI in serum ($n = 10$ mice/group). (*E*) Superoxides produced in the hearts were analysed by staining the ventricular tissues with DHE. (*F*) Immunostaining data of the hearts with 4-HNE antibody were analysed ($n = 3$ mice/group) $^{*}P < 0.05$ vs. WT mice, $^{\dagger}P < 0.05$ vs. 4C30 mice. (*G*) Representative echocardiograms of each group of mice. (*H*) Echocardiographic analysis of cardiac function. (*I*) Kaplan–Meier survival analysis of each group of mice ($n = 25–30$ mice/group).

cardiac muscles and that the surface membrane expression of TRPV2 was decreased by NT domain over-expression. Echocardiography revealed that NT domain over-expression resulted in good amelioration of cardiac dysfunction, with improved FS and EF and reduced fibrosis (*Figure 6C–E*). These results demonstrated that NT domain-induced prevention of the sarcolemmal localization of TRPV2 can greatly ameliorate gene-defective DCM.

3.6 Tranilast prevents cardiomyopathy in J2N-k hamsters

We previously found that tranilast, which is known to be a non-selective cation channel blocker, effectively inhibits TRPV2.[22] Tranilast inhibited 2-APB-induced $[Ca^{2+}]_i$ increases with half-maximal inhibition at about 30 μM, in HEK293 cells expressing TRPV2 (Supplementary material online, *Figure S5*), but it has almost no effect on HEK293 cells expressing TRPV1, TRPV3, or TRPC1 (Supplementary material online, *Figure S5*). A recent study reported that tranilast inhibits TRPV2 ion channel activity.[23] Thus, tranilast is one of the better inhibitors presently available against TRPV2. We observed that tranilast reduced the amount of surface TRPV2 and abnormal Ca^{2+} mobilization by 2-APB in DCM cardiomyocytes (J2N-k, 4C30; unpublished observation). Oral administration of tranilast to J2N-k hamsters resulted in the effective removal of TRPV2 from the sarcolemma of J2N-k hearts (*Figure 6F*), similar to the effect of TRPV2 NT domain over-expression. Tranilast markedly reduced ventricular dilation and muscle fibrosis in J2N-k hearts (*Figure 6G*). Furthermore, it improved cardiac contraction, as evidenced by a decrease in echocardiographic parameters (LVDd and LVDs) to control levels (*Figure 6H*) and improved FS (*Figure 6H*).

4. Discussion

The present results suggest, for the first time, the pathological significance of TRPV2 in DCM development. First, TRPV2 was observed to be extensively localized to the ventricular sarcolemma in DCM patients as well as in animal models of heart failure (J2N-k, 4C30, and DOX-induced cardiomyopathic mice), whereas it localized to the intracellular compartments and intercalated discs in normal ventricles. Second, Tg or adenoviral NT domain over-expression significantly reduced the sarcolemmal accumulation of TRPV2 and simultaneously ameliorated cardiac dysfunction, preventing DCM progression and improving survival in the animal models. Third, the TRPV2 inhibitor tranilast effectively prevented DCM progression in J2N-k hamsters. Based on these findings, we

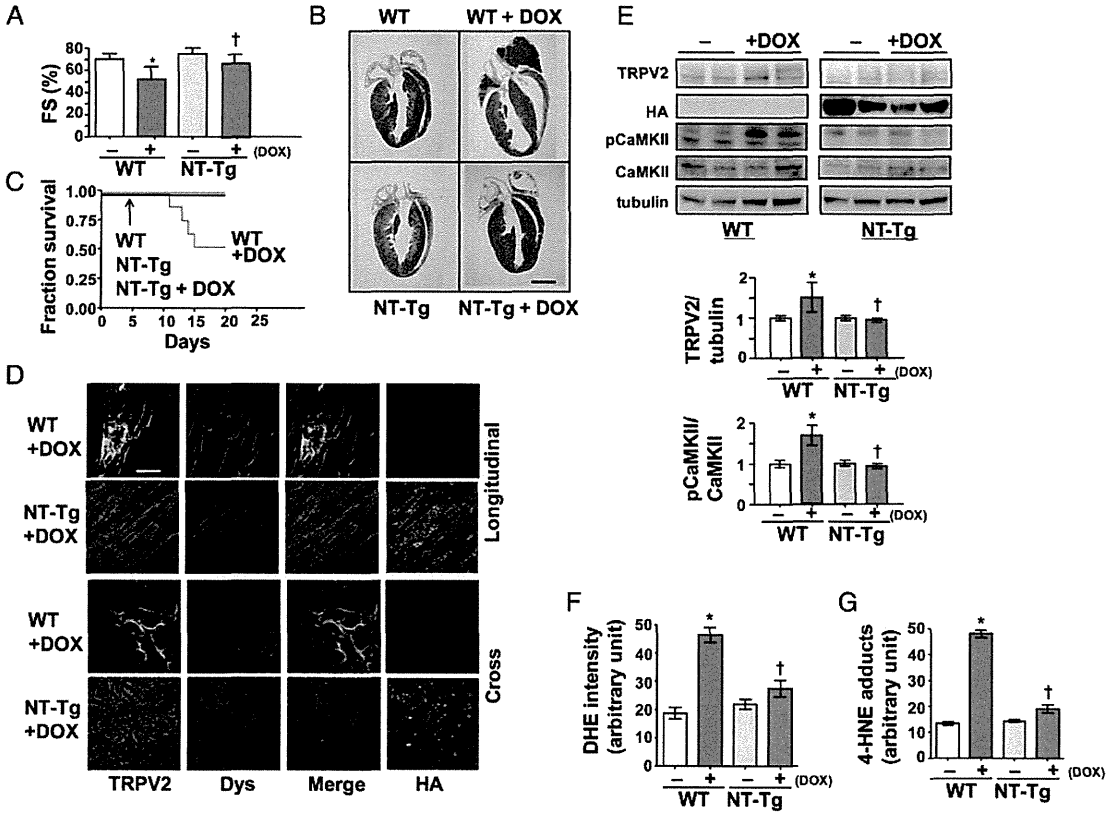

Figure 5 Over-expression of the NT domain ameliorates DOX-induced cardiomyopathy. (*A*) Echocardiographic analysis of cardiac function ($n = 6$ mice/group); $^*P < 0.05$ vs. without DOX, $^\dagger P < 0.05$ vs. WT with DOX. (*B*) Cardiac sections from 11-week-old DOX-treated or untreated WT or NT-Tg mice were stained with Masson's trichrome. Scale bar: 5 mm. (*C*) Kaplan–Meier survival analysis of each group of mice ($n = 15$ mice/group). (*D*) Immunohistochemical analysis of longitudinal (upper panel) and cross-sections (lower panel) of hearts from each group of mice. Scale bar: 100 μm. TRPV2, dystrophin (Dys) and HA antibodies were used. (*E*) Representative immunoblot data of heart homogenates from DOX-treated or untreated WT mice or NT-Tg with the indicated antibodies (left). TRPV2 expression levels are shown relative to tubulin expression and the extent of CaMKII phosphorylation is shown relative to total CaMKII levels (right). The data represent values from three independent experiments. (*F* and *G*) Levels of oxidative stress markers ($n = 4$ mice/group), $^*P < 0.05$ vs. without DOX, $^\dagger P < 0.05$ vs. WT with DOX.

hypothesize that the amelioration of DCM resulted from the inhibition of the Ca^{2+} influx through TRPV2; therefore, TRPV2 may be a potential upstream target against abnormal Ca^{2+} handling.

The DCM phenotype results from a broad variety of primary and secondary aetiologies. Despite the various underlying causes, there are many similarities in the final structural, functional, biochemical, and molecular phenotypes related to the long-lasting mechanical stress and neurohormonal activation observed in DCM.[24] CaMKII is an ideal nodal molecule for transducing Ca^{2+} signals into downstream events such as apoptosis and necrosis, leading to clinical phenotypes of congestive heart failure and sudden death.[25] In addition to CaMKII activation, ROS production is frequently observed in DCM hearts, with detrimental effects on cardiomyocytes.[26] We found that increased CaMKII phosphorylation and ROS production observed in DCM hearts were attenuated by over-expression of the NT domain of TRPV2 (*Figures 4* and *5*), suggesting that TRPV2 may be an upstream regulator of Ca^{2+} influx and ROS production as well as an important mediator of various stress signals, including those arising from genetic defects, mechanical stress, and cardiotoxic drugs, leading to Ca^{2+}-induced cell death. In addition, calcineurin is known to be an important Ca^{2+}-dependent signalling molecule leading to cardiac hypertrophy.[27] Certainly, cardiomyocyte-specific over-expression of calcineurin causes hypertrophy [28] and cardiomyopathy, but conflicting results are reported on the effects of calcineurin inhibition.[29] In our DCM models, calcineurin was slightly activated, as determined by the increase in the expression level of MCIP protein (*Figure 4*) as well as CaMKII activation and inhibition of TRPV2 suppressed both Ca^{2+}-signalling pathways (*Figure 4*). These findings suggest TRPV2 as a putative therapeutic target for the treatment of heart failure.

Here, we used 4C30 mice as a model for human idiopathic DCM. Unlike J2N-k hamsters, which gradually develop DCM, 4C30 mice are apparently asymptomatic up to 100 days but thereafter rapidly exhibit DCM symptoms and die within 200 days. Similar to that in 4C30 mice,[16] sialytransferase expression levels are altered in human DCM.[30] 4C30 mice also show DGC abnormalities (Supplementary material online, *Figure S4*), similar to those in DCM patients (*Figure 2A* and *B*). These characteristics indicate a pointed resemblance between 4C30 mice and human idiopathic DCM. Dystrophin degradation by the Ca^{2+}-dependent protease calpain was proposed as a pathway in

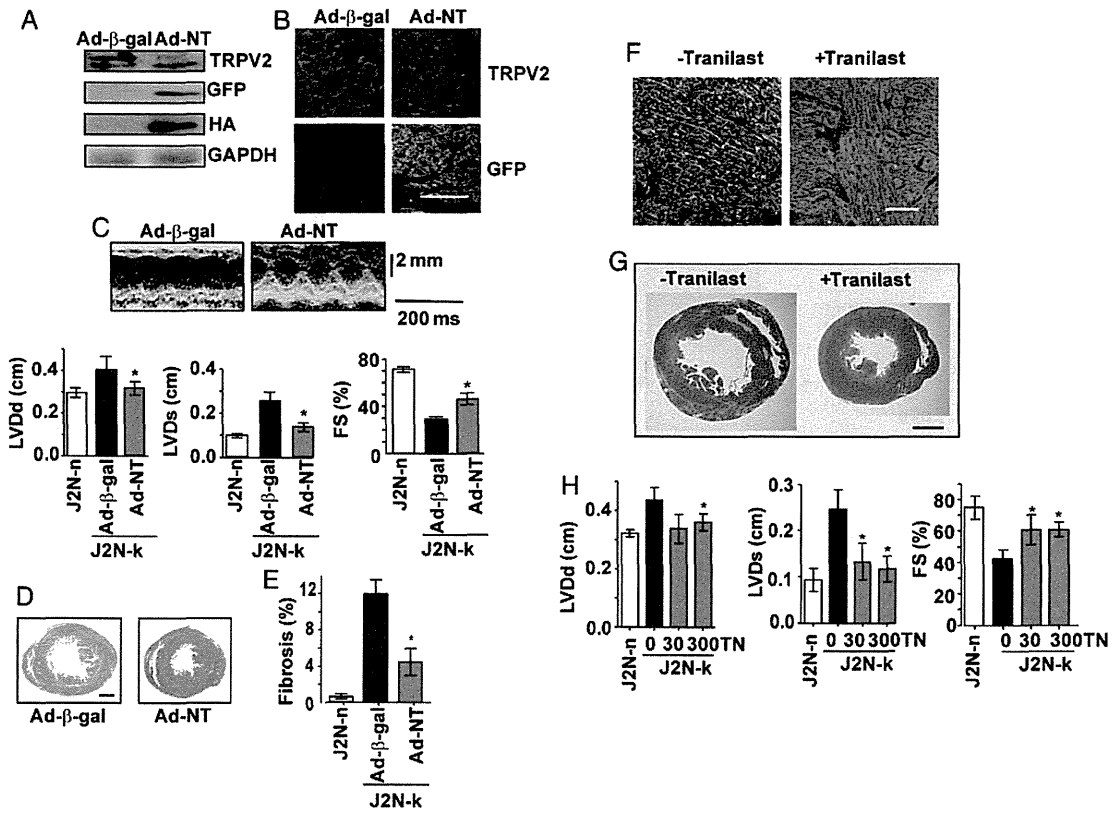

Figure 6 Two inhibitory tools against TRPV2 show comparative amelioration of cardiomyopathy in J2N-k. (*A*) Representative immunoblot and (*B*) immunohistochemical data of heart homogenates or sections from 11-week-old J2N-k infected with adenovirus carrying β-galactosidase (Ad-β-gal, control) or the NT domain (Ad-NT). Adenoviral infection was confirmed by staining with GFP. Scale bar: 100 μm. Similar results were obtained from three independent experiments. (*C*) Echocardiographic analysis of adenovirus-infected J2N-k. Representative echocardiograms (upper panels) and statistical evaluation (lower panels; $n = 6$ hearts/group); $^*P < 0.05$ vs. control. (*D*) Masson's trichrome staining of cardiac sections from adenovirus-infected J2N-k. (*E*) Fibrotic areas were analysed ($n = 6$ hearts/group). (*F*) J2N-k hamsters were administered none (−) or (+) tranilast (300 mg/kg per day) for 2 weeks, and the obtained tissues were immunostained with TRPV2 antibody. Tranilast prevented the sarcolemmal accumulation of TRPV2. Scale bar: 100 μm. (*G*) Heart sections from J2N-k hamsters were stained with Masson's trichrome. Tranilast ameliorated ventricular dilation and reduced fibrosis in these hamsters. Scale bar: 5 mm. (*H*) Effect of tranilast (TN) (0, 30, 300 mg/kg) on echocardiographic parameters in J2N-k ($n = 5$–8 hamsters/group); $^*P < 0.05$ vs. no treatment in J2N-k.

advanced heart failure with DCM symptoms.[31] Therefore, TRPV2 remodelling appears to be linked to sarcolemmal instability caused by DGC defects in various models of advanced heart failure. Thus, the 4C30 mouse appears to be a good animal model to study the connection between Ca^{2+} abnormality and DCM symptoms.

Plasma membrane TRPV2 translocation is known to be stimulated by receptor agonists[15,32] or mechanical stress.[15] Stimulation by growth factors or sympathetic transmitters could act as a signal inducing sarcolemmal TRPV2 translocation in DCM, because these stimulants are known to be released into the blood vessels of diseased hearts in response to mechanical load.[33] Considering that the TRPV2 inhibitory tools abrogated the surface expression of TRPV2 (*Figure 6*), Ca^{2+} influx via TRPV2 may also be important for sarcolemmal TRPV2 accumulation. Although further confirmatory studies are required, we suspect that NT domain over-expression inhibited membrane retention of TRPV2 by disrupting the interaction between TRPV2 and its putative binding partner, which regulates subcellular localization. Recently, a peptide mimetic of the CT domain of connexin 43 was used to disrupt the interaction between connexin 43 and the PDZ2 domain of zonula occludens-1 and reduce gap junction remodelling in injured hearts.[34]

Tranilast prevented ventricular dilation and fibrosis and ameliorated decreased FS by ~50% in J2N-k hamsters (*Figure 6*). These beneficial effects were comparable to those obtained from the adenoviral transfer of the NT domain (*Figure 6*). These treatments were performed in 9-week-old J2N-k hamsters that had already started displaying DCM symptoms. Therefore, our approach may be useful as a therapeutic intervention against the initial symptoms of DCM. Similar results using different strategies (chemical vs. protein) strongly suggest that TRPV2 activity contributes to DCM progression. Importantly, tranilast is immediately available for patients as an anti-inflammatory compound, since it reportedly has anti-inflammatory and immunomodulatory effects;[35] therefore, it may have clinical potential in DCM therapy. Recently, consistent with our data, tranilast has been reported to reduce both functional and structural abnormalities in diabetic cardiomyopathic rats[36] and prevent the progression from compensated hypertrophy to heart failure in pressure-overloaded mice.[37] The latter study suggested that tranilast reduced the heart-failure progression by acting as a mast-cell stabilizer. Since TRPV2 was reported to be involved in mast-cell degranulation,[38] TRPV2 may be also responsible for tranilast-induced amelioration of heart failure.

In conclusion, specific abrogation of TRPV2 activity by either NT domain over-expression or chemical inhibitor treatment led to considerable amelioration of cardiac pathology in the animal models. Our findings strongly suggest that the sarcolemmal TRPV2 accumulation plays a crucial role in Ca^{2+}-induced muscle degeneration in DCM and that TRPV2 is a good therapeutic target for advanced heart failure.

Supplementary material

Supplementary material is available at *Cardiovascular Research* online.

Acknowledgements

We thank Dr Hatsue Ueda (NCVC) for kindly providing us with information for human samples and Dr Yuji Arai (NCVC) for technical support in Tg production.

Conflict of interest: none declared.

Funding

This work was supported by a Grant-in-Aid for Priority Areas (grant number 18077015) to S.W.; Grants-in-Aid (grant numbers 19390080, 17659241 (to S.W.), 18590796, 20590874 (to Y.I.)); and a Grants-in-Aid (grant number 22659046) for Exploratory Research to S.W. from the Japanese Ministry of Education, Culture, Sports, Science and Technology; a grant for the Promotion of Fundamental Studies in Health Sciences of the National Institute of Biomedical Innovation; research grants for Cardiovascular Diseases (grant number 17A-1) to S.W. and Nervous and Mental Disorders (grant numbers 16B-2 and 19A-7) to Y.I. from the Japanese Ministry of Health, Labour and Welfare.

References

1. Hughes SE, McKenna WJ. New insights into the pathology of inherited cardiomyopathy. *Heart* 2005;**91**:257–264.
2. Fatkin D, Graham RM. Molecular mechanisms of inherited cardiomyopathies. *Physiol Rev* 2002;**82**:945–980.
3. Seidman JG, Seidman C. The genetic basis for cardiomyopathy: from mutation identification to mechanistic paradigms. *Cell* 2001;**104**:557–567.
4. Jefferies JL, Towbin JA. Dilated cardiomyopathy. *Lancet* 2010;**375**:752–762.
5. Campbell KP, Kahl SD. Association of dystrophin and an integral membrane glycoprotein. *Nature* 1989;**338**:259–262.
6. Nigro V, Okazaki Y, Belsito A, Piluso G, Matsuda Y, Politano L *et al.* Identification of the Syrian hamster cardiomyopathy gene. *Hum Mol Genet* 1997;**6**:601–607.
7. Jeong EM, Liu M, Sturdy M, Gao G, Varghese ST, Sovari AA *et al.* Metabolic stress, reactive oxygen species, and arrhythmia. *J Mol Cell Cardiol* 2012;**52**:454–463.
8. Toko H, Takahashi H, Kayama Y, Oka T, Minamino T, Okada S *et al.* Ca^{2+}/calmodulin-dependent kinase IIdelta causes heart failure by accumulation of p53 in dilated cardiomyopathy. *Circulation* 2010;**122**:891–899.
9. Beuckelmann DJ, Nabauer M, Erdmann E. Intracellular calcium handling in isolated ventricular myocytes from patients with terminal heart failure. *Circulation* 1992;**85**:1046–1055.
10. Lindner M, Brandt MC, Sauer H, Hescheler J, Bohle T, Beuckelmann DJ. Calcium sparks in human ventricular cardiomyocytes from patients with terminal heart failure. *Cell Calcium* 2002;**31**:175–182.
11. Louch WE, Bito V, Heinzel FR, Macianskiene R, Vanhaecke J, Flameng W *et al.* Reduced synchrony of Ca^{2+} release with loss of T-tubules-a comparison to Ca^{2+} release in human failing cardiomyocytes. *Cardiovascular Research* 2004;**62**:63–73.
12. Eder P, Molkentin JD. TRPC channels as effectors of cardiac hypertrophy. *Circ Res* 2011;**108**:265–272.
13. Nilius B, Owsianik G, Voets T, Peters JA. Transient receptor potential cation channels in disease. *Physiol Rev* 2007;**87**:165–217.
14. Watanabe H, Murakami M, Ohba T, Takahashi Y, Ito H. TRP channel and cardiovascular disease. *Pharmacol Therap* 2008;**118**:337–351.
15. Iwata Y, Katanosaka Y, Arai Y, Komamura K, Miyatake K, Shigekawa M. A novel mechanism of myocyte degeneration involving the Ca^{2+}-permeable growth factor-regulated channel. *J Cell Biol* 2003;**161**:957–967.
16. Suzuki O, Kanai T, Nishikawa T, Yamamoto Y, Noguchi A, Takimoto K *et al.* Adult onset cardiac dilatation in a transgenic mouse line with Galβ1,3GalNAc α2,3-sialyltransferase II (ST3Gal-II) transgenes: a new model for dilated cardiomyopathy. *Proc Japan Acad, SerB* 2011;**87**:550–562.
17. Iwata Y, Katanosaka Y, Arai Y, Shigekawa M, Wakabayashi S. Dominant-negative inhibition of Ca2+ influx via TRPV2 ameliorates muscular dystrophy in animal models. *Hum Mol Genet* 2009;**18**:824–834.
18. Iwata Y, Pan Y, Hanada H, Yoshida T, Shigekawa M. Dystrophin-glycoprotein complex purified from hamster cardiac muscle. Comparison of the complexes from cardiac and skeletal muscles of hamster and rabbit. *J Mol Cell Cardiol* 1996;**28**:2501–2509.
19. Nakamura TY, Iwata Y, Arai Y, Komamura K, Wakabayashi S. Activation of Na^+/H^+ exchanger 1 is sufficient to generate Ca^{2+} signals that induce cardiac hypertrophy and heart failure. *Circ Res* 2008;**103**:891–899.
20. Hu HZ, Gu Q, Wang C, Colton CK, Tang J, Kinoshita-Kawada M *et al.* 2-aminoethoxydiphenyl borate is a common activator of TRPV1, TRPV2, and TRPV3. *J Biol Chem* 2004;**279**:35741–35748.
21. Lievremont JP, Bird GS, Putney JW Jr. Mechanism of inhibition of TRPC cation channels by 2-aminoethoxydiphenylborane. *Mol Pharmacol* 2005;**68**:758–762.
22. Iwata Y, Katanosaka Y, Shijun Z, Kobayashi Y, Hanada H, Shigekawa M *et al.* Protective effects of Ca^{2+} handling drugs against abnormal Ca^{2+} homeostasis and cell damage in myopathic skeletal muscle cells. *Biochem Pharmacol* 2005;**70**:740–751.
23. Mihara H, Boudaka A, Shibasaki K, Yamanaka A, Sugiyama T, Tominaga M. Involvement of TRPV2 activation in intestinal movement through nitric oxide production in mice. *J Neurosci* 2010;**30**:16536–16544.
24. Houser SR, Margulies KB, Murphy AM, Spinale FG, Francis GS, Prabhu SD *et al.* Animal models of heart failure: a scientific statement from the American Heart Association. *Circ Res* 2012;**111**:131–150.

25. Anderson ME. CaMKII and a failing strategy for growth in heart. *J Clin Invest* 2009;**119**: 1082–1085.
26. Giordano FJ. Oxygen, oxidative stress, hypoxia, and heart failure. *J Clin Invest* 2005;**115**: 500–508.
27. Wilkins BJ, Dai YS, Bueno OF, Parsons SA, Xu J, Plank DM *et al.* Calcineurin/NFAT coupling participates in pathological, but not physiological, cardiac hypertrophy. *Circ Res* 2004; **94**:110–118.
28. Molkentin JD, Lu JR, Antos CL, Markham B, Richardson J, Robbins J *et al.* A calcineurin-dependent transcriptional pathway for cardiac hypertrophy. *Cell* 1998;**93**:215–228.
29. Wilkins BJ, Molkentin JD. Calcium-calcineurin signaling in the regulation of cardiac hypertrophy. *Biochem Biophys Res Commun* 2004;**322**:1178–1191.
30. Hwang JJ, Allen PD, Tseng GC, Lam CW, Fananapazir L, Dzau VJ *et al.* Microarray gene expression profiles in dilated and hypertrophic cardiomyopathic end-stage heart failure. *Physiol Genom* 2002;**10**:31–44.
31. Toyo-Oka T, Kawada T, Nakata J, Xie H, Urabe M, Masui F *et al.* Translocation and cleavage of myocardial dystrophin as a common pathway to advanced heart failure: a scheme for the progression of cardiac dysfunction. *Proc Natl Acad Sci USA* 2004;**101**:7381–7385.
32. Kanzaki M, Zhang YQ, Mashima H, Li L, Shibata H, Kojima I. Translocation of a calcium-permeable cation channel induced by insulin-like growth factor-I. *Nat Cell Biol* 1999;**1**: 165–170.
33. Ruwhof C, van der Laarse A. Mechanical stress-induced cardiac hypertrophy: mechanisms and signal transduction pathways. *Cardiovasc Res* 2000;**47**:23–37.
34. O'Quinn MP, Palatinus JA, Harris BS, Hewett KW, Gourdie RG. A peptide mimetic of the connexin43 carboxyl terminus reduces gap junction remodeling and induced arrhythmia following ventricular injury. *Circ Res* 2011;**108**:704–715.
35. Pae HO, Jeong SO, Koo BS, Ha HY, Lee KM, Chung HT. Tranilast, an orally active anti-allergic drug, up-regulates the anti-inflammatory heme oxygenase-1 expression but down-regulates the pro-inflammatory cyclooxygenase-2 and inducible nitric oxide synthase expression in RAW264.7 macrophages. *Biochem Biophys Res Commun* 2008;**371**: 361–365.
36. Kelly DJ, Zhang Y, Connelly K, Cox AJ, Martin J, Krum H *et al.* Tranilast attenuates diastolic dysfunction and structural injury in experimental diabetic cardiomyopathy. *Am J Physiol Heart Circ Physiol* 2007;**293**:H2860–H2869.
37. Hara M, Ono K, Hwang MW, Iwasaki A, Okada M, Nakatani K *et al.* Evidence for a role of mast cells in the evolution to congestive heart failure. *J Exp Med* 2002;**195**: 375–381.
38. Zhang D, Spielmann A, Wang L, Ding G, Huang F, Gu Q *et al.* Mast-cell degranulation induced by physical stimuli involves the activation of transient-receptor-potential channel TRPV2. *Physiol Res* 2012;**61**:113–124.

Clinica Chimica Acta 423 (2013) 10–14

Contents lists available at SciVerse ScienceDirect

Clinica Chimica Acta

journal homepage: www.elsevier.com/locate/clinchim

A prostaglandin D_2 metabolite is elevated in the urine of Duchenne muscular dystrophy patients and increases further from 8 years old

Taku Nakagawa [a], Atsuko Takeuchi [b], Ryohei Kakiuchi [b], Tomoko Lee [a], Mariko Yagi [a], Hiroyuki Awano [a], Kazumoto Iijima [a], Yasuhiro Takeshima [a], Yoshihiro Urade [c], Masafumi Matsuo [d,*]

[a] Department of Pediatrics, Graduate School of Medicine, Kobe University, Chuo, Kobe 6500017, Japan
[b] Kobe Pharmaceutical University, Higashinada, Kobe 6588558, Japan
[c] Department of Molecular Behavioral Biology, Osaka Bioscience Institute, Suita, Osaka 5650874, Japan
[d] Department of Medical Rehabilitation, Faculty of Rehabilitation, Kobegakuin University, Nishi, Kobe 6512180, Japan

ARTICLE INFO

Article history:
Received 25 January 2013
Received in revised form 27 March 2013
Accepted 27 March 2013
Available online 19 April 2013

Keywords:
Tetranor PGDM
Muscle wasting
Inflammation

ABSTRACT

Background: Duchenne muscular dystrophy (DMD) is a progressive muscle wasting disease caused by muscle dystrophin deficiency. Downstream of the primary dystrophin deficiency is not well elucidated. Here, the hypothesis that prostaglandin D_2 (PGD_2)-mediated inflammation is involved in the pathology of DMD was examined by measuring tetranor PGDM, a major PGD_2 metabolite, in urine of DMD patients.
Methods: We measured tetranor PGDM in urine using LC–MS/MS. First morning urine samples were collected from genetically confirmed DMD patients and age-matched healthy controls aged 4 to 15 y.
Results: The urinary tetranor PGDM concentration was 3.08 ± 0.15 and 6.90 ± 0.35 ng/mg creatinine (mean ± SE) in 79 control and 191 DMD samples, respectively. The mean concentration was approximately 2.2-times higher in DMD patients than in controls ($p < 0.05$). Remarkably, urinary tetranor PGDM concentrations in DMD patients showed chronological changes: it stayed nearly 1.5 times higher than in controls until 7 y but surged at the age of 8 y to a significantly higher concentration.
Conclusion: Urinary tetranor PGDM concentrations were shown to be increased in DMD patients and became higher with advancing age. It was indicated that PGD_2-mediated inflammation plays a role in the pathology of DMD.

1. Introduction

Duchenne muscular dystrophy (DMD; OMIM #310200) is the most common inherited muscle disease, affecting one in every 3500 male births and shows progressive muscle wasting resulting in early death. DMD is characterized by muscle dystrophin deficiency caused by mutations in the *dystrophin* gene, which is the largest human gene consisting of 79 exons. DMD patients all carry disastrous mutations in the *dystrophin* gene, such as frameshift or nonsense mutations [1,2]. However, there is some clinical heterogeneity among DMD patients [3,4] and intrafamilial differences have been observed in patients with an identical dystrophin mutation [5]. Dystrophin is a critical member of the dystrophin glycoprotein complex that creates a direct link between the intracellular cytoskeleton and the extracellular matrix of skeletal muscle. The loss of this connection leaves the muscle fibers susceptible to damage resulting in continuous rounds of muscle degeneration/regeneration.

DMD has been classically considered stereotyped in its clinical presentation, evolution, and severity [6–8]. In a minimal disability stage children are without symptoms or with minimal weakness. In the moderate disability stage, patients are impaired in running and climbing stairs. In the severe disability stage, patients are still ambulant but become increasingly handicapped in their physical activities. In the non-ambulant stage that starts before age 12 y, the children are bed-ridden or wheelchair-bound. This progression process has not been totally explained by a primary loss of dystrophin. Inflammatory and immune responses initiated by aberrant signaling in dystrophic muscle have been considered contributors to disease pathogenesis [9].

Prostaglandin (PG) D_2 (PGD_2) has been implicated in both the development and resolution of inflammation. PGD_2 is synthesized by PGD synthase (PGDS) from PGH_2 that is produced from arachidonic acid by the action of cyclooxygenase and 2 PGDS have been disclosed; lipocalin-type PGDS and hematopoietic PGDS (HPGDS)[10,11]. HPGDS in skeletal muscles was found immunohistochemically stained in some of DMD patients but not in controls [12]. This indicated that the inflammatory mediator PGD_2 plays a role in DMD pathology. However, detailed time-course studies of PGD_2 metabolism in DMD patients are incomplete. Recently, urinary 11,15-dioxo-9α-hydroxy-2,3,4,5-

* Corresponding author at: Department of Medical Rehabilitation, Faculty of Rehabilitation, Kobegakuin University, 518 Arise, Ikawadani, Nishi, Kobe 651-2180, Japan. Tel./fax: +81 78 974 6194.
E-mail address: mmatsuo@reha.kobegakuin.ac.jp (M. Matsuo).

0009-8981/$ – see front matter © 2013 Elsevier B.V. All rights reserved.
http://dx.doi.org/10.1016/j.cca.2013.03.031